Master's thesis

NTNU
Norwegian University of Science and Technology
Faculty of Natural Sciences
Department of Chemistry

Seyedmojtaba Seyedraoufi

Studying the optical gaps of retinal *Schiff* base in visual pigments using *ab initio* electronic-structure theory

Master's thesis in Chemistry
Supervisor: Ida-Marie Høyvik
February 2020

NTNU
Norwegian University of
Science and Technology

Seyedmojtaba Seyedraoufi

Studying the optical gaps of retinal *Schiff* base in visual pigments using *ab initio* electronic-structure theory

Master's thesis in Chemistry
Supervisor: Ida-Marie Høyvik
February 2020

Norwegian University of Science and Technology
Faculty of Natural Sciences
Department of Chemistry

NTNU
Norwegian University of
Science and Technology

Abstract

Retina, which is a thin layer of cells in the back of the eyeball, contains two important types of proteins, cone and rod visual pigments. Rod visual pigment or rhodopsin is responsible for vision in low light intensity and cone pigments, consist of red, green, and blue cones, are responsible for day-light vision. All of them contain retinal *Schiff* base as the chromophre and a surrounding protein which tunes the absorption spectrum from 365-430 nm to 498 nm for rhodopsin and 425 nm for the blue cone. Numerous studies, from spectroscopic investigation to theoretical studies devoted to unravel the protein environment role in this significant absorption shift. Electrostatic effect of residues, more importantly the putative counterion of the *Schiff* base, and distortion of the retinal imposed by the protein are well-accepted mechanisms so far provided. Using coupled cluster with approximate singles and doubles method and the resolution of identity approximation (RICC2) as an *ab initio* method together with density functional theory allowed us to dig more into possible role of protein residues rather than the counterion. Our investigation confirms the important role of Glu-113 in rhodopsin absorption. Conversely, in blue cone, deprotonation of the *Schiff* base and group of residues tune the absorption spectrum. We also investigate the effect of different protonation states of Glu-181 and Glu-178 in rhodopsin and blue cone absorption respectively. We conclude that a negatively charged glutamate might disrupt the efficiency of photoisomerization in both pigments. Finally, we investigate the proton affinity of the *Schiff* base in both rhodopsin and blue cone.

Keywords – Rhodopsin, blue cone, RICC2, DFT, excitation energies

Preface

This thesis was a part of Norwegian University of Science and Technology (NTNU)'s two-year master of science program in chemistry (MSCHEM) with specialization in applied theoretical chemistry. this work has been carried out from August 2018 to December 2019 under supervision of associate Professor Ida-Marie Høyvik.

Acknowledgements

I wish to express my special gratitude to my supervisor Ida-Marie Høyvik who patiently helped me to get familiar with quantum chemistry and computational chemistry concepts and her unique and admirable way of supervision and pedagogy incites me to be more passionate about quantum chemistry and electronic-structure theory. I also would like to thank my co-supervisor Henrik Koch and all the people whose assistance was a milestone in the completion of this project. I should mention that the computations carried out in this thesis were performed on resources provided by UNINETT Sigma2 — the National Infrastructure for High Performance Computing and Data Storage in Norway, under project nr nn9409k.

Finally, I would like to thank my mother, Parvin and dedicate this work to my beloved late father Mohsen.

Contents

1 Introduction

Rhodopsin and other cone opsins are light-harvesting proteins playing an important role in visual phototransduction. On the contrary to the rhodopsin, which is the only visual pigment exists in rod cells and is responsible for dim light vision, three different cone pigments, including the blue cone, exist in cone cells and are responsible for day light vision [25]. The struggle to understand how visual pigments interact with light culminates in an electrical impulse and vision has a long history more than a century. However, the topic became more intriguing when it has been cleared that visual pigments are part of interesting G protein-coupled receptors (GPCRs). In fact, rhodopsin is the most studied member of GPCRs family. The machinery of visual pigments is comprised of a protonated or a non-protonated retinal *Schiff* base (RSB) which is entrapped in a delicately-designed protein environment modulating the absorption spectrum of RSB. The *Schiff* base part of retinal is connected to protein from one side and connected to a bulky β-ionine ring via a polyene chain from the other side. Many hydrophilic residues have surrounded retinal (chromophore) which can modulate the optical gap. When exposed to light — for rhodopsin case, it is so sensitive that it can respond to even one photon — RSB undergoes a photoismerization from 11-*cis*- retinal to *all-trans*-retinyldiene which subsequently leads to conformational change of the protein to its active form (metarhodopsin-II). Activated-form will activate a cascade of events results in firing of a neural impulse toward the visual cortex in the brain [25, 39].

One of the outstanding questions regarding visual pigments is how the protein environment tunes the absorption spectrum of retinal from 365-430 nm (2.80-3.40 eV) to 420-560 nm (2.20-2.95 eV) [60]. Studies have suggested two possible mechanisms behind this spectral shift, the electrostatic and polarisation effect of protein residues[31, 36], more specifically the role of Glu-113, and, the steric effect of the protein on the chromophore [28, 60]. However, the first effect has been shown to be more dominant. Supporting the above scenarios, Bravaya et al.[14] have used a quantum mechanical/molecular mechanical (QM/MM) approach in which the QM part was estimated by multiconfigurational quasidegenerate perturbation theory (aug-MCQDPT2). They calculated 599, 448, and 515 nm as the absorption maxima of the retinal *Shiff* base in gas, solution (mixture of water and methanol), and protein environment respectively. They proposed the role of Glu-113 and Glu-181 negative charges and C14-C15 bond nonplanarity inside the protein as the reasons of shift in the absorption spectrum.

Kaila et al.[27] calculated 441 and 491 nm spectral absorbance peaks for blue cone and rhodopsin pigments respectively when applying time-dependent density functional theory (TDDFT), algebraic diagrammatic construction through second order (ADC), and

reduction of virtual space (RVS) approximation method for roughly big cluster models that has been considered fully quantum mechanical. They suggests the electrostatic tuning effect of protein residuals in the proximity of chromophore as the primary effect more dominant to the steric effect of the protein.

In another study, rhodopsin excitation energies have been studied by multireference *ab initio* QM/MM calculations, while putting retinal *Schiff* base in the QM region and the rest of the protein in MM region. According to the results, they postulate that the rest of the protein except Glu-113 does not have any significant effect on the $S_0 \rightarrow S_1$ excitation energy. No charge transfer happening from Glu-113 to the *Schiff* base and that is the reason behind why Glu-113 is omitted from their QM region. And finally, The deprotonation of the *Schiff* base results in significant blue-shifting of the spectrum [7]. The same conclusion has been drawn from another study[45] in which second-order perturbation theory (CASPT2) with atomic natural orbital (ANO) basis set has been applied to calculate excitation energies of retinal embedded within point charges of protein residues calculated at DFT/B3LYP with 6-31G** basis set. Other studies also follow the same foot step for interpretation of the optical shift in rhodopsin [44, 60, 8, 18].

For the blue cone, another effect arises from the deprotonated state of the *Schiff* base. Zhou et al.[60] proposed that significantly lower proton affinity of *Schiff* base inside the blue cone is responsible for its blue-shifted spectrum.

In this study, we calculate the vertical excitation energies of rhodopsin and blue cone different cluster models that have been prepared to elucidate the possible steric and electrostatic role of protein environment. The rhodopsin cluster models prepared from a bovine rhodopsin resolved by x-ray crystallography [38, 60]. For the blue cone we construct our cluster models based on a homology model since no crystal structure was available [49, 60].

The excitation energies will be computed using *ab initio* quantum chemical methods specifically The second-order approximate coupled cluster singles and double (CC2), using the resolution of identity to approximate the two-electron integrals (RICC2). RICC2 method belongs to a successful family of correlated methods named coupled-cluster (CC) theory. The significance of CC methods is related to their exponential ansatz for the wave-function which provides the opportunity to truncate the expansion of the wave-function at certain level. This truncation produces hierarchy of methods with different computational cost that can freely be applied to different systems based on their relative sizes. We also use density functional theory (DFT) with B3LYP functional, and cc-pVDZ basis function for both of calculations.

In the theory chapter, the molecular electronic-structure theories are described in more

details. In the next chapter, prepared molecular models are introduced and more information are provided about computational details. In chapter 4, excitation energies and related interpretations are provided. There is also a subsection about proton affinity of the *Schiff* base in rhodopsin and blue cone. In chapter 5, a conclusion has been drawn, briefing the whole story of the study. And, finally, in section 6, further work has been discussed.

2 Theory

2.1 Many-electron Schrödinger equation

Bearing in mind that solving time-independent Schrödinger eigenvalue equation (TISE) is impossible for multi-electron systems and we need to employ useful approximation to obtain wave-function and/or operators [51]. Slater determinant is a satisfying multiplicative ansatz that pertains anti-symmetric constraint of fermionic wave-function (equation 2.1) [37].

$$\psi(r_1, r_2, ..., r_N) = \frac{1}{\sqrt{N!}} \sum_p (-1)^p \phi_{n_1}(r_1)\phi_{n_2}(r_2)...\phi_{n_N}(r_N). \tag{2.1}$$

In which summation is over all possible permutation of electron indices.

In non-relativistic electronic structure theory we use the molecular electronic Hamiltonian

$$\hat{H} = \hat{T}_e + \hat{V}_{en} + \hat{V}_{ee} + \hat{V}_{nn} \tag{2.2}$$

Where operators are related to kinetic energy of electrons ($\hat{T}_e$), and potential energy provided by electron-nuclei ($\hat{V}_{en}$), electron-electron ($\hat{V}_{ee}$) and nuclei-nuclei ($\hat{V}_{nn}$) interaction. With this approach, the solution of TISE provides us with eigenfunctions that are function of position and spin of the electron (spin-orbitals). To obtain spin orbitals we use set of atomic orbitals (AOs) that are centered on nuclei and are function of position of electron. By assuming AOs as complete set, we can expand the spin orbitals as linear combination of atomic orbitals (LCAOs)[21, 9].

$$\phi_p(r) = \sum_\mu C_{\mu p}\chi_\mu(r) \tag{2.3}$$

Since in practice AOs don't span the whole space, our wave-function is not exact and we need to resort to *the variation principle* to determine expansion parameters (equation 2.3). The variation principle states that the total energy obtained by the variational wave-function is always upper-bound of the exact energy [51].

2.2 Hartree-Fock theory

While working with approximate wave functions, we should consider the variation principle and try to obtain the variational wave-function via minimization of the energy with respect to variational parameters ($\{C_{\mu p}\}$)[51].

To elaborate, it is always more convenient to work with *configuration state functions* (CSFs) instead of Slater determinants since, rather than Hamiltonian, they are at the

same time eigenfunction of the total spin operator and preserves the spin symmetry of the wave-function—their number is also less and/or equal to the number of Slater determinants for a given total projected spin value [21].

Within second quantization formalism, *restricted Hartree-Fock* (RHF) wave-function — in which the α and β spin orbitals are optimized together — can be expressed as a single CSF which constitutes of determinants related by Clebsch–Gordan coefficients[37, 21]. Since in this writing we only work with closed-shell RHF wave-function, CSF is reduced to a single determinant which we refer it to $|cs\rangle$ in following equations. To exploit variation principle, we parameterize our wave-function as a function of unitary transform parameters (κ), then the wave-function can be written as [21]

$$|cs(\kappa)\rangle = \exp(-\hat{\kappa})|cs\rangle \tag{2.4}$$

Where $\hat{\kappa}$ is anti-Hermitian one-electron operator that results in arbitrary rotation of spin-orbitals.

$$\hat{\kappa} = \sum_{p>q} \kappa_{pq}(E_{pq} - E_{qp}) \tag{2.5}$$

Where E_{pq} denotes the singlet excitation operator

$$E_{pq} = a^{\dagger}_{p\alpha}a_{q\alpha} + a^{\dagger}_{p\beta}a_{q\beta} \tag{2.6}$$

Now that we introduced wave-function with variational parameters, we can introduce the energy as expectation value of the wave-function[21]

$$E(\kappa) = \langle cs(\kappa)|\hat{H}|cs(\kappa)\rangle \tag{2.7}$$

Where $\hat{H}$ is electronic Hamiltonian within *Born-Oppenheimer approximation*

$$\hat{H} = \hat{h} + \hat{g} + h_{nuc} = \sum_{pq} h_{pq}E_{pq} + \frac{1}{2}\sum_{pqrs} g_{pqrs}e_{pqrs} + h_{nuc} \tag{2.8}$$

E_{pq} is the singlet excitation operator (equation 2.6) and e_{pqrs} is the two-electron excitation operator

$$e_{pqrs} = \sum_{\sigma\tau} a^{\dagger}_{p\sigma}a^{\dagger}_{r\tau}a_{s\tau}a_{q\sigma} \tag{2.9}$$

The summation in equation 2.8 is over all combination of spin orbitals. And, in equation 2.9, the summation is over spin states (α and β). The excitation operators moves electron(s) from one spin orbital to another without changing the spin state acting on abstract vectors (ON vector) as an abstract representation of Slater determinants. The ensemble of all possible ON vectors constitutes a complete orthonomral basis set called Fock space. h_{pq}

and g_{pqrs} denote one and two-electron integrals which in atomic units are [52]

$$h_{pq} = \int \phi_p^*(r) \left(-\frac{1}{2}\nabla^2 - \sum_I \frac{Z_I}{r_I} \right) \phi_q(r) dr \tag{2.10}$$

$$g_{pqrs} = \int \int \frac{\phi_p^*(r_1)\phi_r^*(r_2)\phi_q(r_1)\phi_s(r_2)}{r_{12}} dr_1 dr_2 \tag{2.11}$$

Where kinetic energy and electron-nuclear interaction are grouped in one-electron integral and electron-electron interaction in two-electron integral. $\phi_i^*(r)$ denotes complex conjugate spin orbital i as function of position of electron (r). Notice that h_{nuc} providing nuclear-nuclear interactions and as a constant just would add to eigenvalues of final equation. [21] Coming back to energy equation of transformed CS (equation 2.7), we can show that by Taylor expansion of energy around $\kappa = 0$ and Baker–Campbell–Hausdorff (BCH) expansion of the Hamiltonian part of $\langle cs| \exp(-\hat{\kappa}) \hat{H} \exp(\hat{\kappa}) |cs\rangle$, the gradient of the energy is equal to

$$\frac{\partial E(\kappa)}{\partial \kappa_{pq}} = \langle cs | [E_{pq} - E_{qp}, \hat{H}] | cs \rangle \tag{2.12}$$

Then our approach is to minimize the expectation value of variational wave-function (equation 2.7) with respect to arbitrary rotation of molecular orbitals. The corresponding equation is

$$\delta E(\kappa) = \delta \langle cs(\kappa) | \hat{H} | cs(\kappa) \rangle = 0 \tag{2.13}$$

When we try to solve the minimization equation via method of *Lagrange multiplier* with orthonormality of spin orbitals as the constraint [51], a one-electron Hermitian singlet operator appears in the equations named as Fock operator. When the Fock operator acts on $|cs\rangle$, forming a pseudo-eigenvalue equation with orbital energies as eigenvalues. However, we call it pseudo since the operator also contains the unknown variational parameters from which the wave-function is constructed. The equation is actually a non-linear equation that can be solved through fix-point iterations named *self-consistent field method* (SCF) [21, 51]. The converged eigenvector is an optimized anti-symmetric closed-shell RHF state named as Hartree-Fock state. To obtain Hartree-Fock energy, we can simply use the optimized $|cs\rangle$ and electronic Hamiltonian and solve the expectation value product to obtain

$$E = 2 \sum_i h_{ii} + \sum_{ij} (2g_{iijj} - g_{ijji}) + h_{nuc} \tag{2.14}$$

Hartree-Fock theory provide us with a good approximation for molecules in equilibrium geometry with significantly lower computational cost in comparison with more advanced

method. However, using a single orbital configuration to define the wave-function neglects electron correlation contribution to the energy which becomes more significant in non-equilibrium geometries [21].

2.3 Coupled-cluster theory

As we mentioned in previous section, The Hartree-Fock theory missing an important piece of contribution, namely electron correlation [9]. Coupled-cluster (CC) theory is a post Hartree-Fock electronic-structure theory which includes description of electron correlation. The CC theory and its application was first brought to realm of quantum chemistry by Cizek and Paldus [15]. Similar to configuration interaction (CI) theory, the CC theory tries to include higher-state determinants in the wave-function, albeit with exponential parameterization — rather than linear parameterization of CI theory.

Thus, we can define the CC wave-function as [24]

$$|CC\rangle = \exp(\hat{T})|HF\rangle \tag{2.15}$$

Where $\hat{T}$ is the cluster operator while acting on HF state, produces different states by distributing electrons among spin orbitals.

$$\hat{T} = \sum_{\mu} t_{\mu}\hat{\tau}_{\mu} \tag{2.16}$$

t_{μ} is corresponding amplitude and $\hat{\tau}_{\mu}$ is the excitation operator.

cluster operator can be defined as the sum of one- two-, ..., N-electron operator that exhibit cluster excitation of electrons

$$\hat{T} = \hat{T}_1 + \hat{T}_2 + ... + \hat{T}_N \tag{2.17}$$

We can define cluster operators ($\hat{T}_1$, $\hat{T}_2$, and so on) in terms of singlet excitation operators by considering the commutability of cluster operator with spin operator [21, 24]

$$\hat{T}_1 = \sum_{ai} t_i^a E_{ai} \tag{2.18}$$

$$\hat{T}_2 = \frac{1}{2}\sum_{abij} t_{ij}^{ab} E_{ai} E_{bj} \tag{2.19}$$

If we write the Schrödinger equation for CC wave-function

$$\hat{H}\exp(\hat{T})|HF\rangle = E\exp(\hat{T})|HF\rangle \tag{2.20}$$

we can derive the (linked) equation for CC energy by left multiplication of equation 2.20 by $\exp(-\hat{T})$ and then $\langle HF|$

$$\langle HF|\exp(-\hat{T})\hat{H}\exp(\hat{T})|HF\rangle = E \tag{2.21}$$

And, we can derive the (linked) amplitude equation of CC theory by left multiplication of equation 2.20 by $\exp(-\hat{T})$ and then $\langle\mu|$ (excited determinant) [15]

$$\langle\mu|\exp(-\hat{T})\hat{H}\exp(\hat{T})|HF\rangle = 0 \tag{2.22}$$

The significance of using linked CC equation is related to BCH expansion of similarity transformed Hamiltonian $\hat{H}^T = \exp(-\hat{T})\hat{H}\exp(\hat{T})$ which is vanishing after few orders depending on the excitation manifold we are using for amplitude equation Thus, the overall number of equations will be reduced which is very helpful while solving non-linear equation with iterative methods [21, 15].

One important point regarding CC theory is the fact that we do not find CC wave-function amplitude variationally. This can be troublesome when we want to derive molecular properties as the Hellmann-Feynman theorem is not fulfilled. To tackle this problem, the CC energy equation is reformulated as the CC Lagrangian. Solving the Lagrangian equation instead of the CC energy equation (equation 2.21) will provide the variational condition. The fulfilment of variational condition will immediately result in the fulfilment of the Hellmann-Feynman theorem [21, 15].

2.3.1 The coupled-cluster singles and doubles (CCSD)

Truncating of cluster operator at second term ($\hat{T}_2$) will lead to the CCSD approximation. We can show that the CC energy equation (equation 2.21) by inserting $\hat{T}_1 + \hat{T}_2$ instead of $\hat{T}$ will turn to

$$E_{CCSD} = E_{HF} + \frac{1}{2}\sum_{aibj}(t_{ij}^{ab} + t_i^a t_j^b)\langle HF|[[\hat{H}, E_{ai}], E_{bj}]|HF\rangle \tag{2.23}$$

and with more simplification we will have

$$E_{CCSD} = E_{HF} + \frac{1}{2}\sum_{aibj}(t_{ij}^{ab} + t_i^a t_j^b)(2g_{iajb} - g_{ibja}) \tag{2.24}$$

that g_{pqrs} is the two-electron integral (equation 2.11) [21].

2.3.2 The second-order approximate coupled cluster singles and doubles (CC2)

Truncation of the cluster operate at a certain excitation would produce hierarchy of CC methods with different scaling in terms of CPU time. Starting from CCS(N^4) — where N denotes the number of orbitals — CCSD(N^6),CCSDT(N^8), and *etc.*, which clearly grows exponentially and rapidly become infeasible for large molecular systems [15]. To alleviate this, CC2 and hierarchy of approximate CC method have been introduced that lies between CC hierarchy based on computational cost, i.e, CC2 scales as N^5 that is between CCS and CCSD [16, 15]. To introduce CC2 equations, it might be a better idea to review the second-order Møller–Plesset perturbation theory (MP2) energy and amplitude equations which provides a good analogy [23].

$$E^{(2)}_{MP2} = \langle HF|\hat{\Phi}\hat{T}^{(1)}_2|HF\rangle = \sum_{aibj} t^{ab}_{ij}\langle HF|\hat{\Phi}|\phi^{ab}_{ij}\rangle \tag{2.25}$$

Where ϕ^{ab}_{ij} denotes doubly excited states and $\hat{\Phi}$ denotes the fluctuation operator. The MP2 amplitudes are given by

$$\langle\phi^{ab}_{ij}|[\hat{F}, \hat{T}^{(1)}_2] + \hat{\Phi}|HF\rangle = 0 \tag{2.26}$$

As we know in MP2 theory, the energy is corrected through second order in the fluctuation potential and the doubly excited states and corresponding amplitudes enters the wave-function as first order in the fluctuation potential [16, 23]. However, following the same line of thought, CCSD energy corrects as third order and singles and triples enters the wave-function [16].

we might write the CCSD amplitude equation as

$$\langle\mu_1|\bar{\hat{H}} + [\bar{\hat{H}}, \hat{T}_2]|HF\rangle = 0 \tag{2.27}$$

$$\langle\mu_2|\bar{\hat{H}} + [\bar{\hat{H}}, \hat{T}_2] + \frac{1}{2}[[\bar{\hat{H}}, \hat{T}_2], \hat{T}_2]|HF\rangle = 0 \tag{2.28}$$

Where $\bar{\hat{H}}$ denotes T_1 transformed Hamiltonian defined as $\bar{\hat{H}} = \exp(-T_1)\hat{H}\exp(T_1)$ and $\{\langle\mu_1|, \langle\mu_2|\}$ represents single and double excitation manifold [16].

To truncate the energy correction at second order in fluctuation potential, we can approximate the doubles amplitude to enter the wave-function as first order similar to MP2 correction. Thus, for doubles equation we have

$$\langle\mu_2|\bar{\hat{H}} + [\hat{F}, \hat{T}_2]|HF\rangle = 0 \tag{2.29}$$

And, we keep singles intact since they don't enter the energy equation and merely improve the quality of the wave-function in terms of orbital relaxation [16]. Orbital relaxation provides opportunity to derive molecular properties, such as excitation energy and frequency-dependent polarizability as it is impossible to derive for MP2 and other many-body perturbation theories [15].

Finally, we might write CC2 energy second-order correction as [23]

$$E^{(2)}_{CC2} = \langle HF|\hat{\Phi}(\hat{T}_2 + \frac{1}{2}\hat{T}_1\hat{T}_1)|HF\rangle \tag{2.30}$$

2.3.2.1 Excited states and energies in the coupled-cluster theory

Excited states and energies can be calculated by two different strategies: *equation-of-motion coupled-cluster* (EOM-CC) and *coupled-cluster response theory (function)* [21, 15]. In EOM-CC, CC optimized wave-function is considered as the reference wave-function from which excited states are generated. It can be considered as CI expansion where the ground states is now optimized CC wave-function [21].

$$|\psi\rangle = \sum_{\mu} c_\mu \hat{\tau}_\mu |CC\rangle = \exp(\hat{T}) \sum_{\mu} c_\mu \hat{\tau}_\mu |HF\rangle \tag{2.31}$$

Since the $|CC\rangle$ are not orthogonal, in formulating of EOM-CC wave-function, a biorthonormal set has been introduced.

$$|\mu) = \exp(\hat{T})\hat{\tau}_\mu |HF\rangle \tag{2.32}$$

$$(\mu| = \langle HF|\hat{\tau}^\dagger_\mu \exp(-\hat{T}) \tag{2.33}$$

Where now we have $(\mu|\nu) = 0$. If we set up the expectation value with our defined wave-functions, we then can define the EOM-CC Hamiltonian matrix with different left and right hand-side equations. It can eventually be shown that excitation energies and coefficients of the excited states can be determined by diagonalization of the *coupled-cluster Jacobian matrix* [16, 21, 30] which can be defined as

$$A_{\mu\nu} = \langle \mu| \exp(-\hat{T})[\hat{H}, \hat{\tau}] \exp(\hat{T})|HF\rangle \tag{2.34}$$

On the other hand, excitation energies and other properties can also be derived from the CC response function regarding a time-dependent perturbing operator—for more information about CC response theory please refer to [30, 16]. In CC response theory, similar to EOM-CC approach, excitation energies are determined as eigenvalues of the

coupled-cluster Jacobian matrix (equation 2.34),

$$AR_m = \omega_m R_m \tag{2.35}$$

Where R_m is right excitation vector contains singles and doubles components. and $(\omega_m = E_m - E_0)$ is the associated excitation energy [24].

2.3.2.2 Oscillator strength

In a special case where the perturbation is related to electromagnetic radiation, oscillator strength is a dimensionless quantity that represents the probability of transition from ground state to excited state. And, can be expressed for $|0\rangle \rightarrow |n\rangle$ transition as [33]

$$f_{0n} = \frac{2m|\mu_{0n}|^2\omega_{n0}}{3e^2\hbar} \tag{2.36}$$

Where m is the electron mass,ω_{n0} is the excitation energy, and $|\mu_{0n}|^2$ is the square modulus of dipole transition. The dipole operator can in the dipole approximation be defined as

$$\hat{\mu} = e\sum_i \vec{r_i} \tag{2.37}$$

The summation is electrons (i) and corresponding distances.

The dipole $|i\rangle \rightarrow |j\rangle$ transition integral can thus be defined as

$$\langle\psi_j|\hat{\mu}|\psi_i\rangle = \int \psi_j^* \hat{\mu}\psi_i dr^3 \tag{2.38}$$

which clearly reveals the importance of wave-function (orbital) overlap of ground and excited state in the intensity of oscillator strength. In CC2 approximation, the dipole transition strength tensor and subsequently oscillator strength are given by

$$S_{0n}^{V^jV^j} = T_{0n}^{V^j} T_{n0}^{V^j} \tag{2.39}$$

Where V^j denotes Cartesian-coordinate component of dipole operator $(j = x, y, z)$ and $T_{0n}^{V^j}$ is constructed from T_1-transformed dipole integrals weighted by left- and right-hand-side eigenvectors of coupled-cluster Jacobian matrix (equation 2.34) and transition moment Lagrangian multipliers. [10]. The CC2 oscillator strength is then given by

$$f_{0n} = \frac{2}{3}\omega_n \sum_{j=x,y,z} S_{0n}^{V^jV^j} \tag{2.40}$$

Which is analogous to general oscillator strength equation (equation 2.36).

2.4 Density functional theory

So far, in non-relativistic electronic structure theory, our approach was to solve the Schrödinger equation by constructing a many-electron wave-function and try to find the approximate wave-function and consequently solution to the equation by exploiting the variation theorem or other techniques. The limitation of this approach becomes more conspicuous when the high number of electrons or large basis sets culminates in a multidimensional complicated wave-function. The least trouble is regarding the implementation in which resultant wave-function imposes high computational cost. An interesting idea is to reduce the many-body wave-function to a three-dimensional electron density [32, 20]. Hohenburg and Kohn [22] theorems are the cornerstones of density functional theory that take the mentioned idea and formulate it suitable for computational chemistry problems.

Briefly, Hohenburg and Kohn theorems postulate that a true density for interacting electrons of a system can uniquely determines the Hamiltonian and properties of the system subsequently. In addition, the energy determined as a function of electron density fulfills the variation theorem.

The significance of Hohenburg and Kohn approach was the formulation of the electron density from one-electron non-interacting orbitals and a universal functional independent of a specific system [32]. When we have a defined electron density, one can set up the self-consistent field equations based on the electron density. However, the the exchange energy definition in universal functional is trivial and need to be obtained by approximation. Local density approximation (LDA), Gradient-corrected approximation (GGA), and the most popular hybrid DFT functional, such as M05-2X and B3LYP, that in derivation using HF exchange definition, are examples of exchange functional approximations already developed.

2.5 Basis sets

As we mentioned in section 2.1, AOs that we are working with, constitutes a finite set of functions, thus the obtained wave-function is not exact even if full expansion is used. These set of functions should be determined priorly. A first reasonable attempt to define this set of functions was to exploit hydrogen atom orbitals. For this purpose, Zener [58] and Slater [48] suggest a set of functions which had the nuclei-electron distance (r) in the exponential. Later on, they have been developed further and named as Slater type orbital (STO) functions. The advantage of STO functions was the fact that they have been originally derived from a real atomic wave-function, thus, provide an excellent description of electron behavior near and far away from nuclei. Near the nuclei ($r \to 0$),

STO functions satisfy nuclear cusp condition, and far away from nuclei ($r \to \infty$) they decay properly [35]. Unfortunately, STO function popularity plummeted very fast since two-centered integrals formulated by STO functions turned out to be very hard to solve analytically.

Gaussian type orbital (GTO) introduced by Boys [13] and McWeeny [34] as an alternative set of functions to improve two-centered integral problem of STOs. AS a property, the product of two Gaussian functions centred on two points in space can be reduced to one Gaussian placed on the line connecting the two points [35]. This property solves the integral problem of STOs. However, GTOs are not satisfying nuclear cusp, and decay very fast in comparison with STO functions. All in all, computational easiness of GTOs provoked researchers to develop and implement it far more than STOs.

To grasp the correlation energy, new set of GTOs introduced that exponential parameter has been optimized with respect to correlation energy. The most prevalent sets were suggested by Dunning and the famous one cc-pVDZ proposed for the atoms placed at second row elements. Here, cc-p denotes *correlation consistent* polarized. DZ stands for double-ζ meaning that two GTOs with different ζ parameters assigned to each of occupied atomic orbital. And, V, denotes that just valence electrons will be treated [52, 35].

3 Molecular systems and computational details

3.1 Rhodopsin molecular models

The best structure of rhodopsin available is 2.2 Ångstrom resolution of Bovine rhodopsin that has improved structural features, such as pre-twist of the C11-C12 double bond of chromophore (PDB: 1U19) [38]. We have obtained a model system prepared upon 1U19 which is comprised of 400 atoms in which the amino acids cut and saturated by hydrogen at C_β atoms and structurally optimized at DFT/BP86 level with def2-SVP basis sets and RI-MARIJ approximation. During optimization, retinal and hydrogens of the first surrounding layer of residues let to be relaxed [60]. we will refer this model as RH400 in this writing. This model system is still large enough to render *ab initio* quantum chemical computations highly expensive. To overcome this problem, we tried to narrow down the big model to smaller models centered around *11-cis*-retinal *Schiff* base (RSB) as the chromophore. To break down the big model, we used our chemical intuition and previous literature indicating that electrostatic effect of protein residues, such as glutamate 113 (Glu-113) and glutamate 181 (Glu-181), and structural strain effect exerted by protein environment play pivotal role in spectral tuning of RSB [27, 14, 8]. Bearing these facts in mind, we designed our model systems by including the RSB as the chromophore, its putative counterion (Glu-113) [38, 27, 14, 8], Glu-181, two water molecules (Wat2a and Wat2b), and a protonated imidazole ring pertains to His-211 (figure 3.1). His-211 is protonated [38] in dark state and during activation and conformational change of protein (metarhodopsin-II) becomes deprotonated [40].

One question may arise here: on which base we have truncated the RH400 model system and what are the criteria to do so? The decision-making process in which molecule should be included was based on two factors, the significance of their effects on excitation energy of chromophore that reported in literature and their distance with respect to the chromophore [60, 27, 14, 8, 44]

Electrostatic interaction is a long-range inter-molecular interaction and can exert significant effect at long distances but we have kept to a range of 10 Å to include all charged molecules within this range in our model systems [59].

Useful to say here that, according to RH400 model, we can detect a hydrogen-bonded network (HBN) in the vicinity of *Schiff* base which has wrapped around negatively charged carboxylate group of Glu-113 and Glu-181. The HBN is comprised of two water molecules (Wat2a and Wat2b) and hydroxyl group of Ser-186 that stabilize the peculiar deprotonated

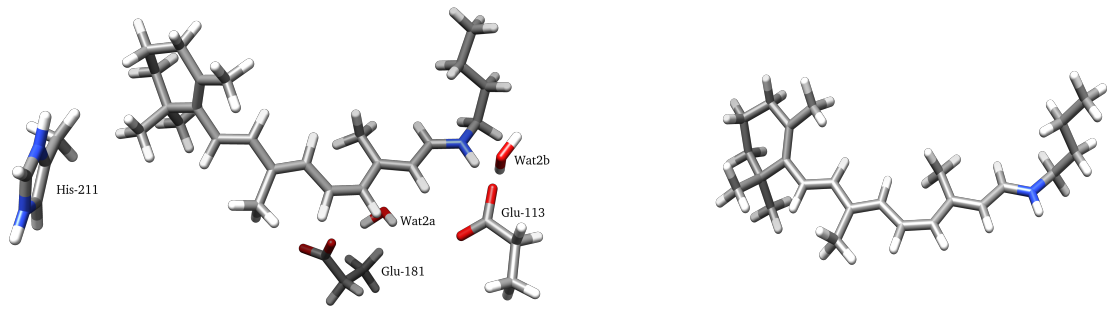

(a) **(b)**

Figure 3.1: (a) Protonated retinal *Schiff* base (have been referred to as SBH-RH400) surrounded by important residues obtained from RH400 model. (b) Gas phase fully relaxed protonated retinal *Schiff* base structure (have been referred to as SBH *in vacuo* in this writing) [60]. You can see the β-ionine ring on the left of the molecule and protonated *Schiff* base on the right.

form of Glu-113. According to [38], the HBN might also be responsible for conformational change of RSB in metarhodopsin-I state that turn Glu-181 to a new counterion for the *Schiff* base. However, we know that there is a controversy over protonation state of Glu-181 in the dark state [18, 19]. and we will discuss it later in section 4.5.2.

3.1.1 SBH-GLU181, SBH-GLU113, and SBH-HIS211 cluster models

To investigate possible role of Glu-113, Glu-181, and His-211 on the chromophore excitation energies, we prepared simple cluster models. Notice that, our simplest cluster model here is protonated retinal *Schiff* base (SBH-RH400) that has been obtained by removing all protein residues except the chromophore from RH400 model. The second model is SBH-GLU181 which contains SBH-RH400 and Glu-181. SBH-GLU113 model includes SBH-RH400 and Glu-113, and the last one is SBH-HIS211 which includes SBH-RH400 and His-211 (figure 3.1).

3.1.2 SGW and SGHW cluster models

Following the same priciple, we construct two more models: SGW that includes SBH-RH400, Glu-113, and two water molecules (Wat2a and Wat2b). And, SGHW which includes SBH-RH400, Glu-113, His-211, and wat2b. SGW has been made to evaluate the role of water molecules and Glu-113 on the excitation energies and possible shielding effect of waters on Glu-113 negative charge. And, SGHW to investigate His-211 effect on the excitation energies (figure 3.1).

3.1.3 SBHcarb(0)imd(0) and SBHcarb(0)imd(+)

To explore the possible effect of His-211 protonation states on the chromophore, we prepared two cluster models: SBHcarb(0)imd(0) and SBHcarb(0)imd(+), where sign inside the parentheses implies the charge associated with each of the residues. Both of them are comprised of SBH-RH400, Glu-181 in its protonated form (carb(0)), and Glu-113 in its deprotonated form. The only difference is related to His-211 protonation state—imd(0) is the deprotonated form and imd(+) is the protonated form (figure 3.1). We calculated first excitation energy of SBHcarb(0)imd(+) at RICC2/cc-pVDZ level. Then, we removed the proton from the nitrogen inside the imidazole ring and optimized the nitrogen bonds at DFT/B3LYP level while keeping the rest of the model fixed in their positions.

3.1.4 Cluster models to investigate different protonation states of Glu-181

Here we produced 8 different cluster models to evaluate the effect of protonation states of Glu-181 on the optical gap of SBH-RH400 as the chromophore. The models are SBcarb(-), SBcarb(0), SBcarb(-)imidwaters, SBcarb(0)imidwaters, SBHcarb(-), SBHcarb(0), SBHcarb(-)imidwaters, SBHcarb(0)imidwaters. Where SBH and SB denotes protonated and deprotonated retinal *Schiff* base respectively. carb(0) and carb(-) stands for protonated and deprotonated form of Glu-181 (charge of the carboxylate group determined in parentheses) and finally, imidwaters denotes imidazole ring of His-211 and two water molecules (figure 3.1).

3.2 Blue cone molecular models

The blue cone structure has been elucidated by a homology model [49](PDB: 1KPN). We obtained a truncated model system of it which consists of 356 atoms, and again, the amino acids cut and saturated by hydrogen at C_β atoms — we will refer to it as BL400 for convenience [60]. Because of the size of the system we have the same story regarding computational cost, therefore we fragmented it into smaller model systems based on aforementioned criteria. We have carboxylate group (which we refer it as Glu-110 in the blue cone pigment) and *Schiff* base that are closely juxtaposed. However, we have different proportions of protonated (SBH) and deprotonated (SB) form of RSB in BL400 rather than RH400, and we will discuss it further in section 4.7.

Comparing with RH400 and related model systems, differences come in when we arrive at HBN: the water molecules have been substituted with the hydroxyl group of Ser-183 that stabilizes Glu-110, and, the phenolic group of Tyr-265 and the indolic group of trp-188

that stabilize the other negatively charged carboxylate group that for this model pertains to Glu-178. The other interesting difference is related to the phenolic group of Tyr-262 that has popped up in the middle of protein cavity in the vicinity of β-ionine ring (figure 3.2) [49].

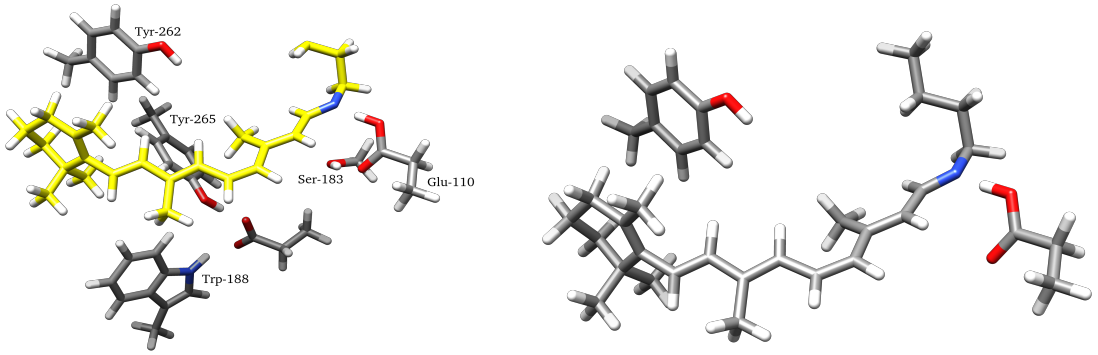

(a) **(b)**

Figure 3.2: (a) deprotonated retinal *Schiff* base (refer as SB-BL400 in this writing and colored in yellow in this picture) surrounded by important residues obtained from BL400 model. (b) SGT cluster model which includes SB-BL400, Tyr-262, and Glu-110

3.2.1 SB-BL400, SG, and SGT cluster models

To understand the modulatory effect of Glu-110 and Tyr-262 on the absorption spectrum of deprotonated retinal *Schiff* base inside the BL400 model, we construct SB-BL400, SG, and SGT cluster models. SB-BL400 is just deprotonated retinal *Schiff* base according to coordinates from BL400 model. SG constitutes SB-BL400 and Glu-110, and in SGT, as it is clear from figure 3.2, we add Tyr-262 to SG model.

3.2.2 Cluster models to investigate different protonation states of Glu-178

Glu-178 has two possible protonation states together with two possible retinal *Schiff* base (SB and SBH), we construct 4 cluster models: SBcarb(-), SBcarb(0), SBHcarb(-), SBHcarb(0). SB and SBH denotes deprotonated and protonated retinal *Schiff* base. carb(0) and carb(-) stands for protonated and deprotonated Glu-178 (figure 3.2). Notice that the protonation state of the *Schiff* base and counterion (here is Glu-110) is coupled together meaning that the proton is moving from one to another due to the very close distance.

3.3 Computational details

While investigating different protonation states, we performed geometry optimization of protons and affected atoms and/or residues while fixing the rest of atoms at DFT/B3LYP level of theory and cc-pVDZ as basis set using Northwest Computational Chemistry Package (NWChem) 6.8 [53]. NWChem uses the quasi-newton method [17], and maximum and root mean square of gradient and iteration step to define the convergence criteria [3]. In our calculations, to reduce the excessive computational cost, we also accept the optimization while the energy gradient has been close enough to zero (quantitatively while the $dE \approx 10^{-5}$). We should notice that RSB excitation energies are dependent on the ground state geometry. We chose B3LYP functional for our geometry optimizations since the associated excitation energies show a good agreement with experiment and/or high level *ab initio* methods [55].

An extensive benchmarking study regarding basis-set dependency of RICC2 excitation energies of different biochromophores has been conducted by Send et al.. One of the chromophore is retinal *Schiff* base of rhodopsin which is optimized at MP2/TZVP level with resolution-of-identity approximation. Basis sets are comprised of double-, triple-, and quadruple-ζ Karlsruhe basis sets (def2-SVP, def2-TZVP, and def2-QZVP), and, the augmented triple-ζ correlation-consistent basis set (aug-cc-pVTZ). The basis-set convergence of the lowest excitation energy (eV) shows the following trend, 2.23, 2.17, 2.16, and 2.15 for def2-SVP, def2-TZVP, def2-QZVP, and aug-cc-pVTZ respectively [46]. Inserting our calculated lowest excitation energy at RICC2/cc-pVDZ level, 2.19 eV, reveals a less than 0.1 eV basis-set dependency of retinal *Schiff* base excitation energies. This value is an acceptable error and encouraged us to use cc-pVDZ basis set to reduce the cost of our computations.

Coupled-cluster and DFT calculation of the excitation energies performed through LSDalton 1.0, an electronic structure program [6]. Regarding the RICC2 calculation, we exploit the frozen-core approximation and the convergence threshold for Frobenius norm of the SCF (self-consistent field) gradient [2] was set to 10^{-5}. For some of the calculations, to reduce cost of the computation, we also exploit correlated natural transition orbital frame-work for low-scaling excitation energy calculations (CorNFLEx), which is using the active orbital space determined at CIS level then calculating excitation energy at the CC2 level [11].

For the pKa calculation we used Schrödinger 2019-4 software and its Jaguar package which use DFT energy and empirical parameters to calculate approximated pKas [4, 12, 57, 29]. we will discuss more about Jaguar scheme for pKa calculation and our approach to calculate approximated values for retinal *Schiff* base pkas in section 4.7.

Molecular graphics and analyses including natural transition orbitals (NTOs) and electrostatic potential plots (MEPs), performed with UCSF Chimera [41]. NTOs were plotted with a contour value of 0.03 a.u, and for colored-surface ESP maps we set the color-associated values from -0.03 (for the lowest ESP associated with higher electron density) to 0.03 (for the highest ESP) in standard rainbow palette coloring.

To perform our calculations we used UiT (University of Tromsø – The Arctic University of Norway) high performance computing Stallo cluster [5].

4 Results and discussion

Our approach here is to first explore the ground state electrostatic potential plots of different protonation states of RSB with and without its counterion to reveal the ground-state charge distribution along the molecule. At the same time, we calculate related excitation energies which gives us an opportunity to suggest possible interpretation for observed shifts in the chromophore absorption. In section 4.2, we try to address the steric contribution of protein to the overall spectrum shift of the chromophore. Then, in the next section, we evaluate the possible electrostatic contribution of different residues on RSB excitation energies. We also consider different protonation states of Glu-181 in rhodopsin model (figure 3.1) and Glu-178 in blue cone model (figure 3.2) in section 4.5.2. Finally, we will try to answer an important question of why RSB is deprotonated in blue cone and protonated in rhodopsin.

4.1 RSB ground and excited states exploration

In order to explore the possible role of RSB-surrounded residues and/or functional groups in excitation energy and absorption spectrum of chromophore, it is better to start with the simplest model which usually provides us with the most understandable information. These information can later be used as the basis to understand more complicated model systems. To do so, we cut out, by retaining the conformation, the deprotonated RSB (SB) from RH400 model (RET-RH400). Then we calculate the excitation energies (usually the first two ones) at RICC2/cc-pVDZ level. And, finally, we calculate the ground state electrostatic potential (ESP) at DFT/B3LYP level and plot electrostatic potential map (MEP). We started comparison by adding a proton to *Schiff* base and completed it by adding the counterion (Glu-113: SB(-)).

4.1.1 Electrostatic potential maps

Before considering excitation energies, we might scrutinize ground state MEPs. In figure 4.1, we can see the charge distribution along the SB molecule in its ground-state wave function. A concentration of negative charge centered on the *Schiff* base that diminishes gradually as we move toward the β-ionine ring is noticeable. Conversely, we have deprivation of electron density close to the β-ionine ring and on the edge of the molecule where we do not have the extension of conjugated π orbitals. In the next step, we add the Glu-113 to the model and plot MEP this time with color-associated values ranging from -0.2 to 0.2. The effect of closing negatively charged carboxylate group toward *Schiff* base is dispersing the electron density from nitrogen to the β-ionine ring through conjugated π orbitals based on correlation effects of electrons.

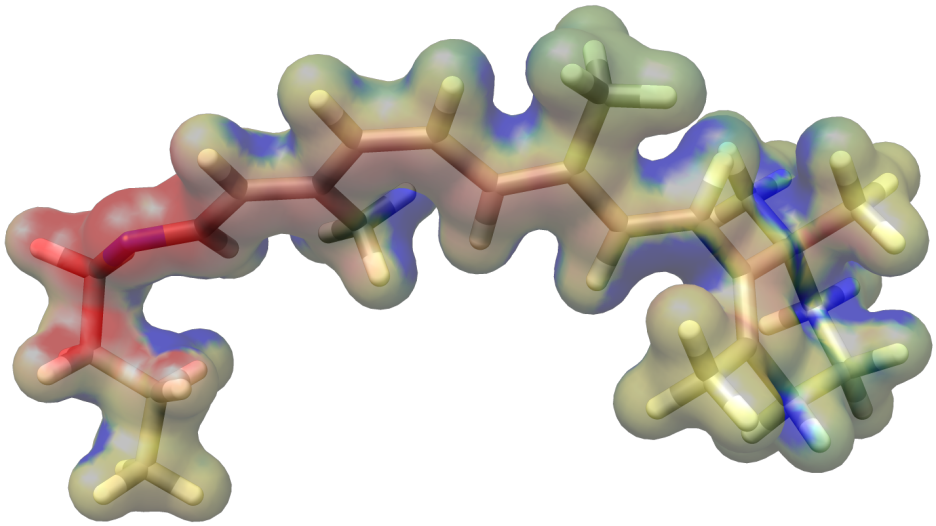

Figure 4.1: Electrostatic potential map of SB ground state. We used UCSF Chimera 1.13.1 to produced colored-surface ESP maps and set the color-associated values from -0.03 (for the lowest ESP associated with higher electron density) to 0.03 (for the highest ESP) in standard rainbow palette coloring.

However, as we can see in figure 4.2, the correlation effect cannot entirely overcome the electron-nuclear attraction, and we still have considerable amount of excessive electron density around the *Schiff* base. This remained excessive charge can lead to a significant destabilization of SB(-) ground state in comparison with SB ground state.

Moving forward, we added a proton to the nitrogen, and based on our previous observation about SB charge distribution, we can predict that adding proton to *Schiff* base is going to stabilize the SBH ground state in comparison with SB and of course SB(-). In figure 4.2 (c), we observe an almost even distribution of excessive positive charge — brought to the system by the proton — across the molecule by the means of conjugated π orbitals. But the most interesting model is when we add Glu-113 with its negative charge juxtapose to *Schiff* base (figure 4.2 (d)). Unexpectedly, we see the same charge distribution as we observed for SB(-) model, we have high electron density around nitrogen atom that diffuses via conjugated π orbitals. However, since our molecule has overall positive charge, we can detect excessive positive charge on the edge of the molecule and close to the β-ionine ring. One possible interpretation for this peculiar behavior might be related to the very close distance of Glu-113 and *Schiff* base (1.5 Å) that led to sharing electron density from carboxylic acid to *Schiff* base. But, regardless of the exact mechanism, we can draw the same conclusion as we had for the SB(-) model system: adding Glu-113 to SBH has led to a destabilization of ground state.

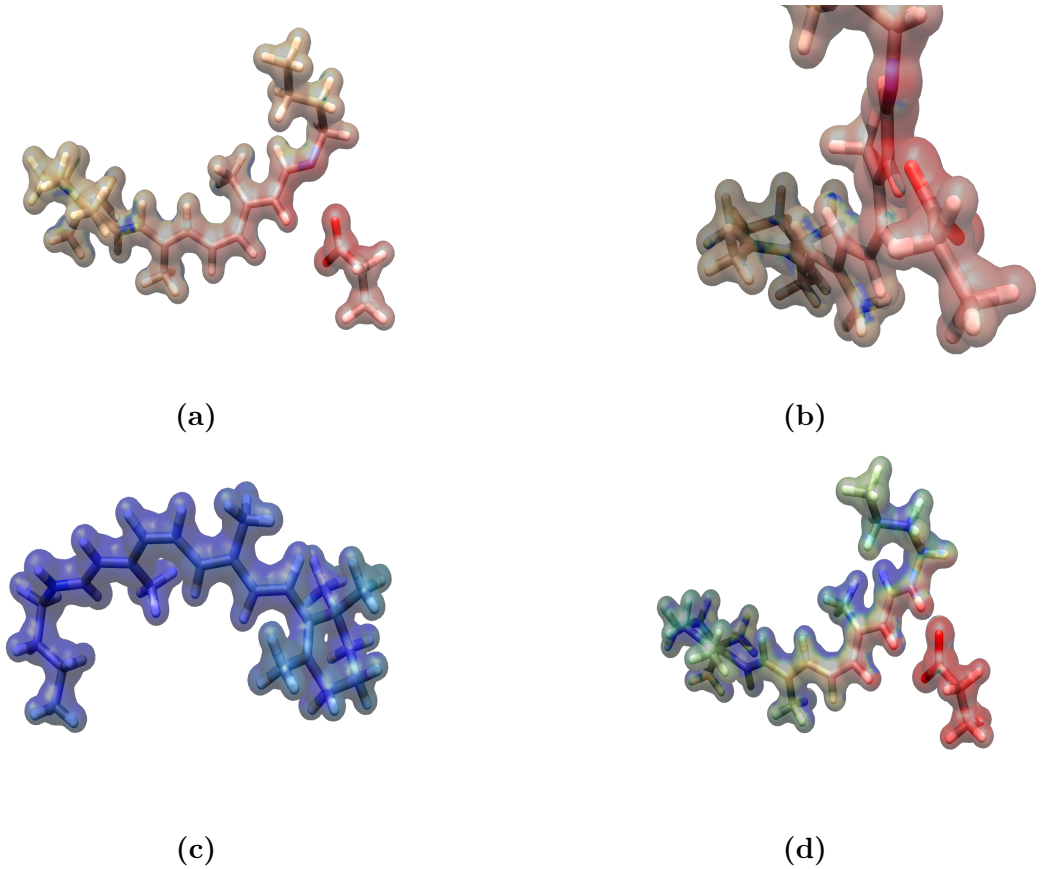

Figure 4.2: (a) Electrostatic potential map (MEP) of SB(-) ground state. (b) closer look at the effect of negative charge on the *Schiff* base electron density. We set the color-associated values from -0.2 (for the lowest ESP associated with higher electron density) to 0.2 (for the highest ESP) in standard rainbow palette coloring. (c) MEP of SBH ground state. We set the color-associated values -0.03, -0.015, 0, 0.05, and 0.1 in standard rainbow palette coloring. (d) MEP of SBH(-) ground state. We set the color-associated values from -0.03 to 0.03 in standard rainbow palette coloring.

4.1.2 Excitation energies

Now that we have an acceptable picture of our basic model systems (SB, SB(-), SBH, and SBH(-)) ground state energy, we can take a look at the excitation energies.

In table 4.1, we can see the first and second excitation energies for four possible combinations. SB has the highest excitation energy, and adding proton (SBH) and Glu 113 (SB(-)) has significantly reduced it. Seeking for a better picture, we first plot natural transition orbitals (NTOs) of excited states calculated at RICC2/cc-pVDZ level of theory. Then, we try to combine the results that we got from aforementioned ground states study to have a more comprehensive explanation for table 4.1 excited state energies. If we compare SB with SBH model, we already know that SBH ground state has been stabilized by the proton that we add to *Schiff* base (figure 4.2 (c)). However, when we inspect NTOs of SB and SBH, we observe a clear movement of electron density from excited

MODEL	RICC2 1st [eV]	f	RICC2 2nd [eV]	f
SB	3.394	1.845	3.565	0.075
SBH	2.172	1.405	3.243	0.387
SB(-)	1.190	0.014	1.939	0.010
SBH(-)	2.565	0.008	2.833	0.538

Table 4.1: RICC2/cc-pVDZ first and second excitation energies of RET-RH400 basic models with associated oscillator strength (f).

conjugated π^* orbitals to the *Schiff* base (figure 4.3). Thus, a reasonable interpretation is that adding proton has stabilized excited state more than it stabilizes the ground state.

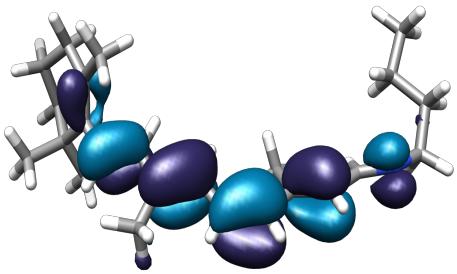

(a)

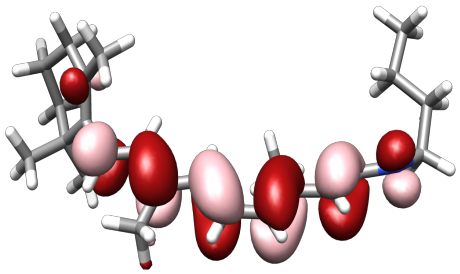

(b)

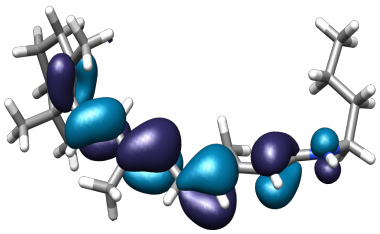

(c)

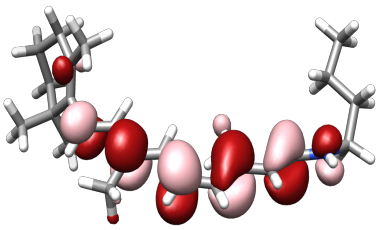

(d)

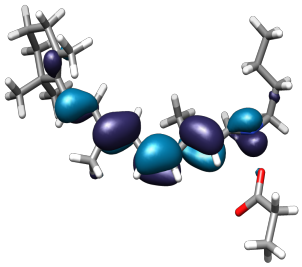

(e)

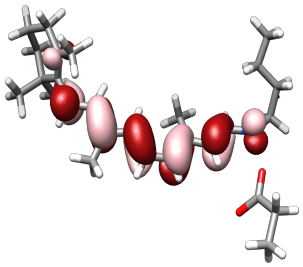

(f)

Figure 4.3: Stick representation of the SB and SBH molecule. Natural transition orbitals for lowest excitation are plotted with a contour value of 0.03 a.u. (a) SB occupied NTO. (b) SB virtual NTO. (c) SBH occupied NTO. (d) SBH virtual NTO. (e) SB(-) occupied NTO. (f) SB(-) virtual NTO.

Applying the same line of though, by considering NTOs of SB and SB(-) (figure 4.3) we might conclude that Glu-113 has destabilized ground state and excited state, but not at the same pace, it has destabilized ground state more than excited state.

Combination of above scenarios should be used to explain SBH(-) excitation energy meaning that the proton has stabilized both states and Glu-113 has destabilized them (figure 4.4). However, it is hard to say which process is dominant. Thus, we should add one more possible condition to the two above mentioned ones: destabilization of ground state and stabilization of excited state which also leads to the same result.

(a) **(b)**

Figure 4.4: Stick representation of the SBH(-) molecule. Natural transition orbitals for lowest excitation are plotted with a contour value of 0.03 a.u. (a) occupied NTO. (b) virtual NTO.

4.2 Steric tuning of rhodopsin and blue cone

Before introducing the RH400 cluster models and compare them with their counterparts in BL400 models, it is useful to see the role of strain that induced by protein on the RSB. We know that rhodopsin and blue cone proteins as an environment induce strain elicit deformation of RSB relative to its *in vacuo* conformation. Here, we would like to compare the excitation energies of SB and SBH fully relaxed *in vacuo* with their constrained form inside the protein pocket. If we look at $S0 \rightarrow S1$ excitation energy of SBH-RH400 versus SBH *in vacuo*, it is conspicuous that protein environment does not have significant effect on the energy gap. This result conveys another important conclusion that "opsin shift" should stem from naked residues surrounding the RSB [8] — more specifically the so-called counterion of *Schiff* base.

In other words, "steric tuning" is not dominant in SBH-RH400 model. And as we said, residues that cover the protein pocket and not being shielded by any solvent should play

MODEL	RICC2 1st [eV]	f	RICC2 2nd [eV]	f
SBH-RH400	2.172	1.405	3.243	0.387
SBH *in vacuo*	2.190	1.727	3.388	0.473
SB-BL400	3.551	1.836	4.028	0.001
SB *in vacuo*	3.723	2.022	4.336	0.001

Table 4.2: Comparing first and second excitation energies and oscillator strength (f) of protonated retinal *Schiff* base obtained from RH400 model (SBH-RH400) and depreotonated retainal *Schiff* base that obtained from BL400 (SB-BL400) with fully relaxed *in vacuo* SB and SBH conformations.

MODEL	EE[a] [eV]	EE[b] [eV]	EE[c] [eV]	Experiment [eV]
SBH-RH400	2.17	2.11	2.09	2.03
SBH *in vacuo*	2.19	2.13	2.27	-
SB-BL400	3.55	3.41	2.90	-
SB *in vacuo*	3.72	3.58	3.05	-

Table 4.3: Comparing vertical excitation energies (EE) of protonated (SBH) and deprotonated (SB) retianl *Schiff* base fixed in the protein pocket versus fully relaxed *in vacuo* conformation. (a) Excitation energies at RICC2/cc-pVDZ level. (b) Excitation energies at RICC2/aug-cc-pVDZ level: augmented basis sets used only for carbon and nitrogen. (c) Excitation energies at FDET/TDDFT (B3LYP/DZP) level [60]. All fully relaxed structures obtained by DFT/B3LYP geometry optimization.

more important role. However, in SB-BL400 model, steric tuning effect on absorption spectrum is much more considerable and red-shifted the absorption energies 0.16 eV (averaged on different calculation methods). This result is in accordance with other cone pigment absorption studies [60].

4.3 RH400 cluster models excitation energies

Coming back to rhodopsin and RH400 model system to reiterate that so far we tried to pinpoint important residues — exceptions are water molecules that we only have them in RH400 — that reportedly [60, 27, 14, 8, 44] have significant effect on RSB excitation energies and/or our chemical intuition persuade us to include them in our cluster models. Starting from Glu-113, water molecules and the protonated imidazole ring of His-211 (figure 3.1).

We have tabulated different cluster models made from RH400 model (table 4.4). Clearly, Glu-113 has widened optical gap of chromophore (SBH-RH400), and it is clear by comparing SBH-GLU113 and SBH-RH400 which is in accordance with our result and suggested possible explanation at section 4.1.2. If we compare SBH-GLU113 with SGW (SBH plus Glu-133 plus water molecules), we will arrive at another interesting conclusion: water molecules blue-shifting effect. We know that water molecule, as an important part

MODEL	CCS first [eV]	CCS second [eV]	RICC2 first [eV]	RICC2 second [eV]
SBH-GLU181	3.044	3.193	-1.061 (0.000)	-0.386 (0.000)
SBH-GLU113	3.458	5.237	2.373 (0.030)	2.702 (0.056)
SGW	3.436	5.222	2.805 (0.429)	2.872 (1.202)
SGHW	3.500	5.290	2.626 (–)	2.959 (–)
SGHW (CorNFLEx)	–	–	3.02 (1.733)	4.449 (0.235)
SBH-HIS211	3.220	4.997	2.336 (1.471)	3.458 (0.336)
SBH-RH400	3.141	4.872	2.172 (1.406)	3.243 (0.388)

Table 4.4: Comparing first and second excitation energies of different cluster models of RH400 at CCS/cc-pVDZ and RICC2/cc-pVDZ level with oscillator strength in parentheses. SGHW denotes Glu-113, His-211, and water moleculre (Wat2b).

of HBN, stabilize negative charge of Glu-113 carboxylate group and with this phenomenon ensure the stability of protonated form of retinal *Schiff* base (SBH) inside the rhodopsin [38]. We also know that HBN is responsible for hydrolysis and release of SBH from protein cavity in metarhodopsin-II state [26]. However, we can now observe the possible blue-shifting role of water molecule in rhodopsin absorption spectrum. We can explain this observation with the same interpretation we proposed in section 4.1.2. Meaning that the water molecule shields the destabilizing effect of Glu-113 negative charge by formation of the hydrogen bond. By alleviation of the narrowing effect of on the energy gap, we can see a blue-shifting result of water molecule which is close to Glu-113.

Another interesting result, by comparing SBH-HIS211 with SBH-RH400, is from positively charged imidazole which is placed at the proximity of β-ionine ring which has resulted in blue-shifting for both first and second excitations. This is in accordance with Zhou et al. claim that any positive charge near β-ionine ring will result in blue-shifting effect on the spectrum. However, we cannot confirm their proposed mechanism that this result is due to stabilizing the ground state. Our result — by investigating NTOs of excited states and MEPs of ground states — clearly showed the depletion of electron density from β-ionine ring toward the *Schiff* base. This means that adding a positive charge close to β-ionine ring would destabilize both states; however, it should destabilize the excited state more than the ground state. We can see in our SGHW model the blue-shifting effect in comparison with SBH-RH400. However, we didn't see any synergistic blue-shifting while comparing with SGW which was not predictable. To address this inconsistency, we calculate the excitation energy of SGHW model, this time with correlated natural transition orbital frame-work for low-scaling excitation energy calculations (CorNFLEx). We used this method since it produced the same excitation energies in comparison with RICC2 but at lower computational cost. The result is now consistent with our interpretation and shows a synergistic blue-shifting effect. When we add Glu-181 to our SBH model, we came across an unexpected huge energy shift that we could not explain it by our methodology and other related studies [60, 27, 47, 54]. We try to address this problem in more details

MODEL	DFT first [eV]	DFT second [eV]	RICC2 first [eV]	RICC2 second [eV]
SB-BL400	2.915 (1.399)	3.419 (0.001)	3.551 (1.836)	4.028 (0.001)
SG	2.778 (1.305)	2.960 (0.006)	3.366 (1.759)	4.413 (0.297)
SGT	2.736 (1.194)	2.943 (0.003)	3.322 (1.638)	4.347 (0.336)

Table 4.5: Comparing first and second excitation energies of different cluster models of BL400 at DFT/B3LYP and RICC2/cc-pVDZ level with associated oscillator strength in parentheses. SG denotes *Schiff* base of BL400 and Glu-110, and SGT denotes *Schiff* base, Glu-110 and Tyr-262.

in section 4.5.2.

4.4 BL400 cluster models excitation energies

Regarding BL400, we prepared a model includes RSB, Glu-110, and Tyr-262. In table 4.5, we have reported first and second excitation energies of SB-BL400, SG (denoting deprotonated BL400 *Schiff* base, and protonated Glu-110) , and SGT (includes BL400 *Schiff* base, Glu-110 and Tyr-262) that have been calculated at RICC2/cc-pVDZ and DFT/B3LYP level (figure 3.2). As we can see, Glu-110 has red-shifted deprotonated RSB — which is the common form inside the blue cone — absorption spectrum. The important observation here is the role of Tyr-262 in decreasing the excitation energies — while comparing SG and SGT energies. Notice that Tyr-262 was not present at RH400 model.

4.5 Protonation states of ionizable residues in RH400 and BL400

Since we have included three ionizable side chain (Glu-133, Glu-181, and His-211) in our cluster models, it is reasonable to study the possible effect of different protonation states of these residues on RSB absorption spectrum. To do so, at first step, we try to address His-211 protonation states effects and then we introduce more complicated combination of cluster models to investigate different protonation states of Glu-113 and Glu-181 in RH400 model, and Glu-110 and Glu-178 in BL400 model.

4.5.1 His-211 protonation state in RH400

For His 211, we have produced two cluster models (SBHcarb(0)imd(0) and SBHcarb(0)imd(+)) based on our explanation at section 3.1 (3.1), and listed them in table 4.5. The result shows that deprotonated imidazole ring leads to a more blue-shifting ($\simeq 0.14eV$), comparing with SBH-GLU113 model in table 4.4, than protonated imidazole. This is quite interesting since the imidazole ring considered as electron deficient ring and

we are still destabilizing excited state more than ground state based on our discussion at section 4.1.2. However, it seems that a milder electron-deficient residues (imidazole vs. protonated imidazole) in the vicinity of β-ionine ring would increase the energy gap.

MODEL	CCS first [eV]	CCS second [eV]	RICC2 first [eV]	RICC2 second [eV]
SBHcarb(0)imd(0)	3.42	5.19	2.79	2.90
SBHcarb(0)imd(+)	3.48	5.27	2.65	2.94

Table 4.6: Comparing first and second excitation energies of two identical model with different protonation states of His-211.

4.5.2 GLU-181 and Glu-178 different protoantion states

The main goal of this section is to address the effects of different protonation states of Glu-181 and Glu-178 on RSB optical gap in RH400 and BL400 respectively. Four different cluster models have been prepared from BL400 model (figure 3.2) including SBcarb(-), SBcarb(0), SBHcarb(-), SBHcarb(0) (carb(-) denotes ionized Glu-178 and carb(0) denotes protonated Glu-178). Following the same procedure, eight cluster models prepared for RH400 model (3.1), SBcarb(-), SBcarb(0), SBcarb(-)imidwaters, SBcarb(0)imidwaters, SBHcarb(-), SBHcarb(0), SBHcarb(-)imidwaters, SBHcarb(0)imidwaters. Here "imidwaters" denotes protonated imidazole ring of His-211 and two water molecules (section 3.1).

As we mentioned earlier, when we have deprotonated Glu-181 and Glu-178 as its counterpart in BL400 model, we stumble across a significant shift in excitation energies which seems to be out-of-trend results. To resolve this problem, we decided to inspect NTO plots associated with higher excitation energies for each of the cluster model. We expected that first and second most important excitations with highest amplitudes are dominated by excitations that engaged conjugated π orbitals. However, it was not the case when we inspect the excitations of clusters including bare Glu-181 in rhodopsin and blue cone models. A question may arise here: how can we select appropriate excitation energies for each cluster model that can be comparable and/or interpretable?

To answer this question, we define a procedure with specific criteria by which one can determine the most appropriate excitation in accordance with our photoisomerization process. We know that during the photoisomerization process *11-cis* retinal convert to *all-trans* retinal. Thus, a successful excitation produces an excitation state in which C11-C12 double bond weakened and reduces the activation energy for rotation around the bond.

At first step, we plot NTO for each of the excitations in the order of importance that they have been produced. Then, we select the earliest that shows the proper movement of

electron density based on above criterion. For the excitations that more than one pair of orbital has the significant amplitude to contribute, we inspect a linear combination of NTOs. However, we should emphasize that this procedure just provide us with a qualitative determination of excitation energies that by combination of related oscillator strength can give us a probable absorption spectrum for each of the cluster model.

4.5.2.1 BL400 cluster models

Starting form BL400 cluster models, we have arranged excitation energies (mostly first ten excitations) that have obtained at RICC2/cc-pVDZ and DFT/B3LYP level of theory (table 4.7 and table A1.1 in the appendix). When we changed the protonation state of each one of the cluster models, we optimized the protons, nitrogen of *Schiff* base, and carboxylate group. We also let water molecules to be optimized while we fixed the rest of the system.

Starting with SBcarb(-) of BL400 would be a good example of the way we approached to excitation energies problem. In figure 4.5 we have plotted first 6 NTO plots that obtained at DFT/B3LYP level. As you can see, the first to sixth are the excitations that engaged occupied orbitals of Glu-181 and virtual ones of RSB. According to our selection criteria, we should neglect these excitations. The 8^{th} NTO is presenting our excitation of interest since it significantly removes electron density from C11-C12 double bond and increase the probability of a photoisomeization event. It is not surprising that this excitation has the largest dominant oscillator strength since in this case conjugated π orbitals are engaged in excitation and we have a significant occupied-virtual orbital overlap.

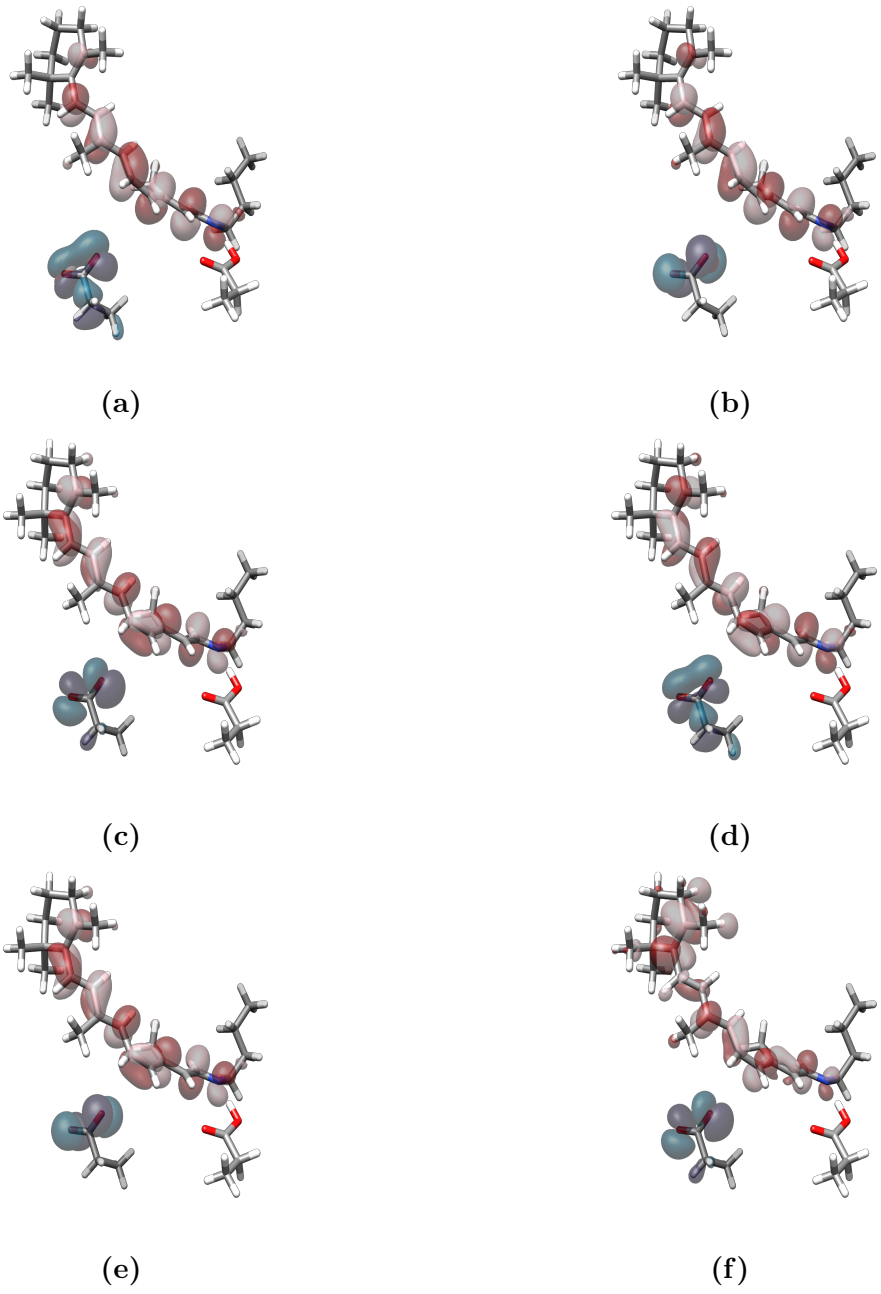

Figure 4.5: Stick representation of the SBcarb(-) molecular model. Natural transition orbitals for lowest DFT/B3LYP excitation are plotted with a contour value of 0.03 a.u. (a) First excitation (b) Second excitation (c) Third excitation (d) Fourth excitation (e) Fifth excitation (f) sixth excitation.

We also have plotted the NTOs generated based on CCS as a guide to determine appropriate excitations. The first NTO seems to be a suitable excitation that efficiently removes the C11-C12 electron density. Furthermore, we also have excitation number three which seems to remove density properly with lower transition probability.

For number 1 and 3 the program has generated more than one NTO which shows more than one excitation has relatively high amplitude. The 6^{th} NTO is representing an

(a) **(b)**

Figure 4.6: Stick representation of the SBcarb(-) molecular model. Natural transition orbitals for 8^{th} DFT/B3LYP excitation are plotted with a contour value of 0.03 a.u. (a) Occupied NTO. (b) Virtual NTO.

inappropriate excitation; however, if we correlate it to RICC2 excitation energies, then it has the highest oscillator strength.

As an interpretation to this observation we might say that NTOs obtained from CCS level indicates that the lowest excitation is the appropriate one. However, it has a close-to-zero oscillator strength indicating a very low electric dipole transition strength or occupied-virtual orbital overlap. This inconsistency can be related to our truncated molecular model and/or using CCS NTOs (since we don't see the same problem in DFT generated NTOs). Notice that NTOs were generated at CCS level, then, excitation energies calculated at RICC2 level and it was assumed that the order of excitation energies have been retained. Considering above mentioned observation, this assumption might not be true.

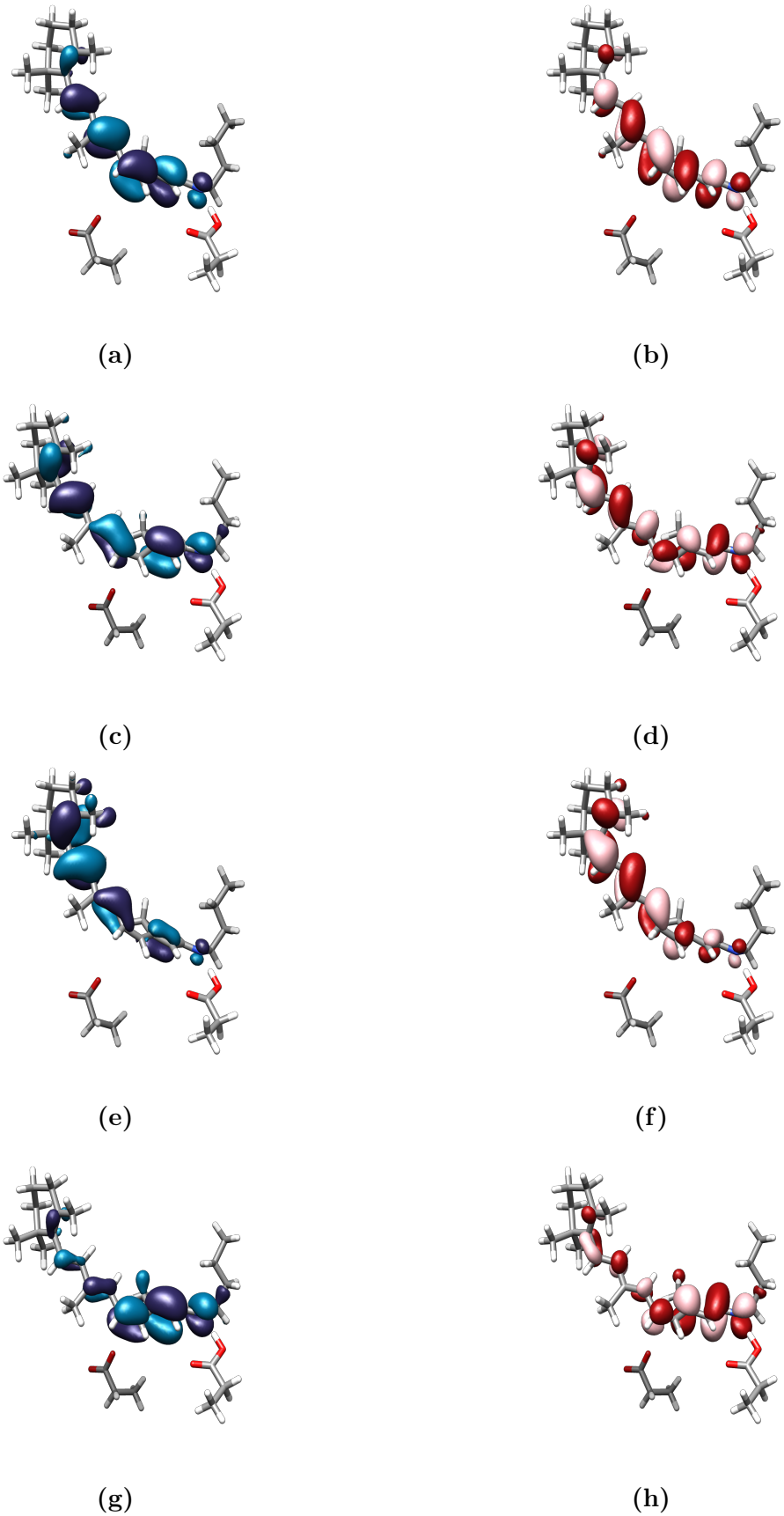

Figure 4.7: Stick representation of the SBcarb(-) molecular model. Natural transition orbitals for lowest CCS/B3LYP excitation are plotted with a contour value of 0.03 a.u. (a) First excitation occpied NTO (b) First Excitation virtual NTO (c) Second important occupied NTO contributing to 1^{st} excitation (d) Second important virtual NTO contributing to 1^{st} excitation (e) 3^{rd} excitation occupied NTO (f) 3^{rd} excitation virtual NTO (g) and (h) second important NTOs contributing to 3^{rd} excitation.

(a) **(b)**

Figure 4.8: Stick representation of the SBcarb(-) molecular model. Natural transition orbitals for 6^{th} CCS/cc-pVDZ excitation are plotted with a contour value of 0.03 a.u. (a) Occupied NTO. (b) Virtual NTO.

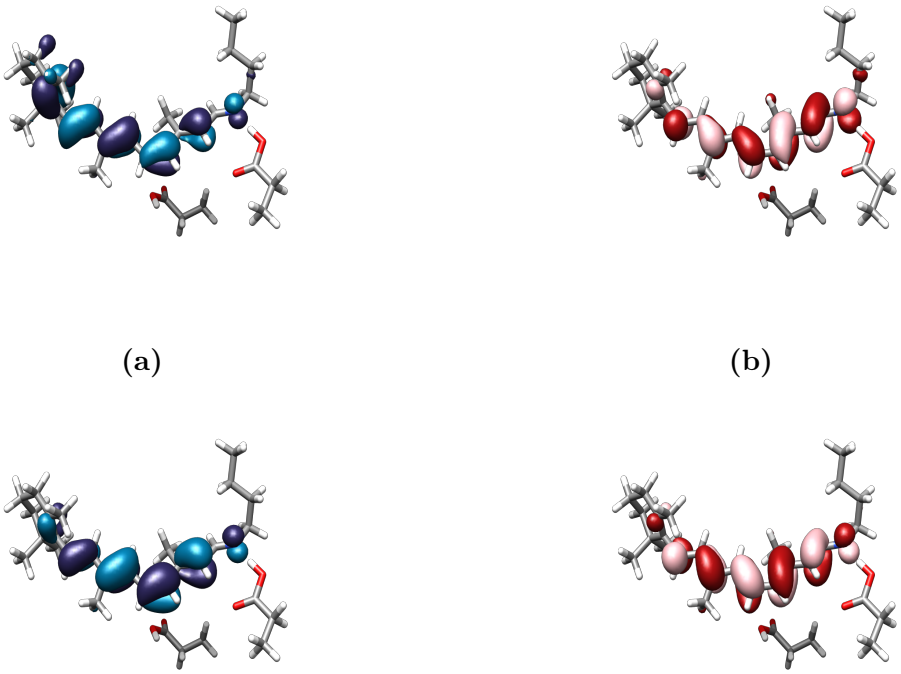

(a) **(b)**

(c) **(d)**

Figure 4.9: Stick representation of the SBcarb(0) molecular model. Natural transition orbitals for 1^{st} CCS/cc-pVDZ excitation and DFT/B3LYP are plotted with a contour value of 0.03 a.u. (a) DFT occupied NTO (b) DFT virtual NTO (c) CCS occupied NTO (d) CCS virtual NTO.

Moving to SBcarb(0) cluster model, which as clear in figure 4.9, NTO plots of first excitation from both DFT and CCS passed our criteria. This observation might have

fruitful consequences useful to solve the controversy over protonation states of Glu-181. We will discuss it further at the end of this section.

In SBHcarb(-) model, our RSB is now in its protonated form. Inspecting NTOs generated via DFT, we notice excitation number 10 without an entirely dominant oscillator strength is removing electron density properly (figure 4.11). On the other hand, situation for CCS plots is not as clear as DFT plots. In figure 4.10 we have plotted number 7 second important NTO which is demonstrating a proper excitation. However, the first important 7^{th} excitation was not a proper one. We chose number 7 since the lower ones were not relevant for mediating a cis-trans isomerization (weakening the double bond).

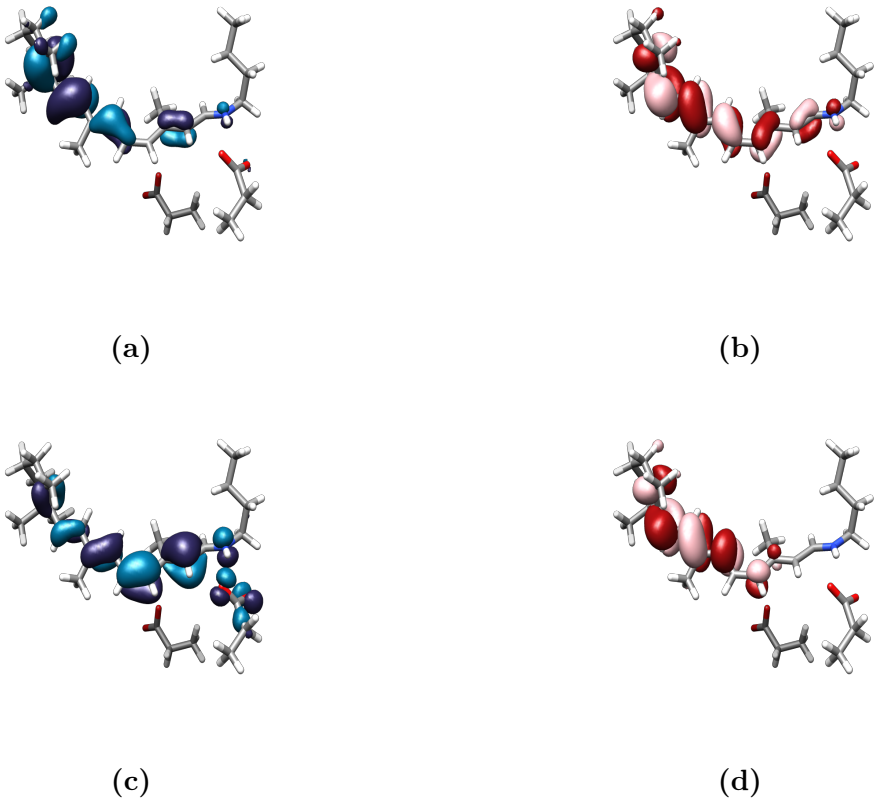

(a) **(b)**

(c) **(d)**

Figure 4.10: Stick representation of the SBHcarb(-) molecular model of blue cone. Natural transition orbitals for fifth and seventh CCS/cc-pVDZ excitations are plotted with a contour value of 0.03 a.u. (a) fifth occupied NTO (b) fifth virtual NTO (c) seventh occupied NTO (d) seventh virtual NTO.

(a) **(b)**

Figure 4.11: Stick representation of the SBHcarb(-) molecular model of blue cone. Natural transition orbitals for 10th DFT/B3LYP excitations are plotted with a contour value of 0.03 a.u. (a) tenth occupied NTO (b) tenth virtual NTO.

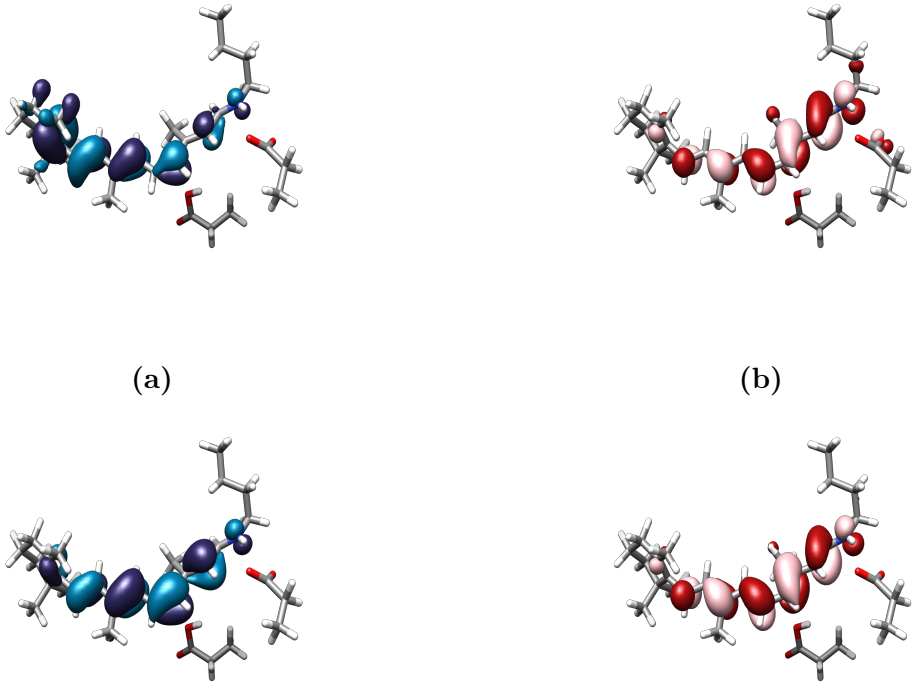

(a) **(b)**

(c) **(d)**

Figure 4.12: Stick representation of the SBHcarb(0) molecular model of blue cone. Natural transition orbitals for 5th DFT/B3LYP excitation and 1st CCS/cc-pVDZ are plotted with a contour value of 0.03 a.u. (a) Fifth DFT occupied NTO (b) Fifth DFT virtual NTO (c) first CCS occupied NTO (d) first CCS virtual NTO.

For SBHcarb(0), which is the last cluster model of BL400, we plotted the fifth excitation of DFT based NTOs and first excitation of CCS based NTOs that show relevant excitation

Blue cone models	RICC2 [eV]	f	DFT [eV]	f
SBcarb(-)	1.391	0.000	2.863	1.482
SBcarb(0)	3.416	1.772	2.815	1.326
SBHcarb(-)	2.643	0.000	2.714	0.602
SBHcarb(0)	1.853	0.027	2.577	0.755

Table 4.7: Selected relevant excitation energies and associated oscillator strength (f) of blue cone Glu-110 and Glu-178 different protonation states calculated at RICC2/cc-pVDZ and DFT/B3LYP level of theory.

for mediating the photoisomerization in figure 4.12. All selected relevant first excitation energies of above-discussed cluster models of blue cone are listed in table 4.7. For complete table of excitation energies please refer to table A1.1 in the appendix.

4.5.2.2 RH400 cluster models

Following the same procedure as BL400 models, we start with SBcarb(-). First excitation of CCS plots and 10^{th} excitation of DFT plots were the ones that remove electron density properly. For SBcarb(0) cluster model, we have the same scenario as we had for the counterpart in blue cone, the lowest excitation with the highest oscillator strength were the relevant ones (table 4.8 and table A2.1 in the appendix).

For SBcarb(0)imidwaters, we observed again the lowest excitation of CCS and tenth excitation of DFT plots were appropriate ones. However, for SBcarb(-) the irrelevant excitations were the ones that engaged Glu-181 orbitals, but in SBcarb(0)imidwaters, we don't have the same problem since we have protonated Glu-181 indicating that we don't have the conjugated π orbital in the carboxylate group of Glu-181 anymore. Without this conjugated orbital structure, it seems that we don't have significant orbital overlap between Glu-181 π orbitals and long conjugated π orbitals of retinal polyene. Instead of that, now we have another conjugated π orbital related to imidazole ring that has a good overlap as we can see in figure 4.13.

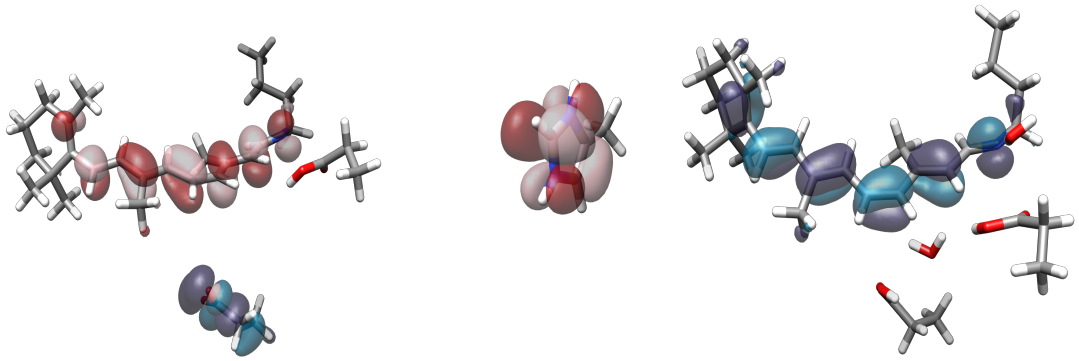

(a) **(b)**

Figure 4.13: Stick representation of the SBcarb(-) and SBcarb(0)imidwaters molecular models of rhodopsin. Natural transition orbitals for improper excitations are plotted with a contour value of 0.03 a.u. (a) First excitation (DFT) of SBcarb(-): occpied NTO (blue) and virtual NTO (red). (b) First excitation (DFT) of SBcarb(0)imidwaters, occpied NTO (blue) and virtual NTO (red).

For Sbcarb(-)imidwaters, based on our above-mentioned line of thought, the irrelevant orbital overlaps are now more frequent since we have both negatively charged Glu-181 and imidazole ring. That is why we found the excitation number 19 as the relevant excitation. But, surprisingly, we could find the relevant excitation as the first excitation based on CCS plots. Moving to SBHcarb(-), we found number 5 as the relevant excitation for CCS plots. However, based on DFT plots, we found 9^{th} excitation as the relevant one.

In SBHcarb(0) model, excitation number one is the relevant one based on CCS plots and relate them to RICC2 excitation energies (table 4.8). However, if we inspect DFT NTOs we notice that for instance first excitation has engaged Glu-113, which now is negatively charged, and conjugated π orbitals of retinal polyene (figure 4.14). That is why we couldn't find the relevant excitation earlier than number four.

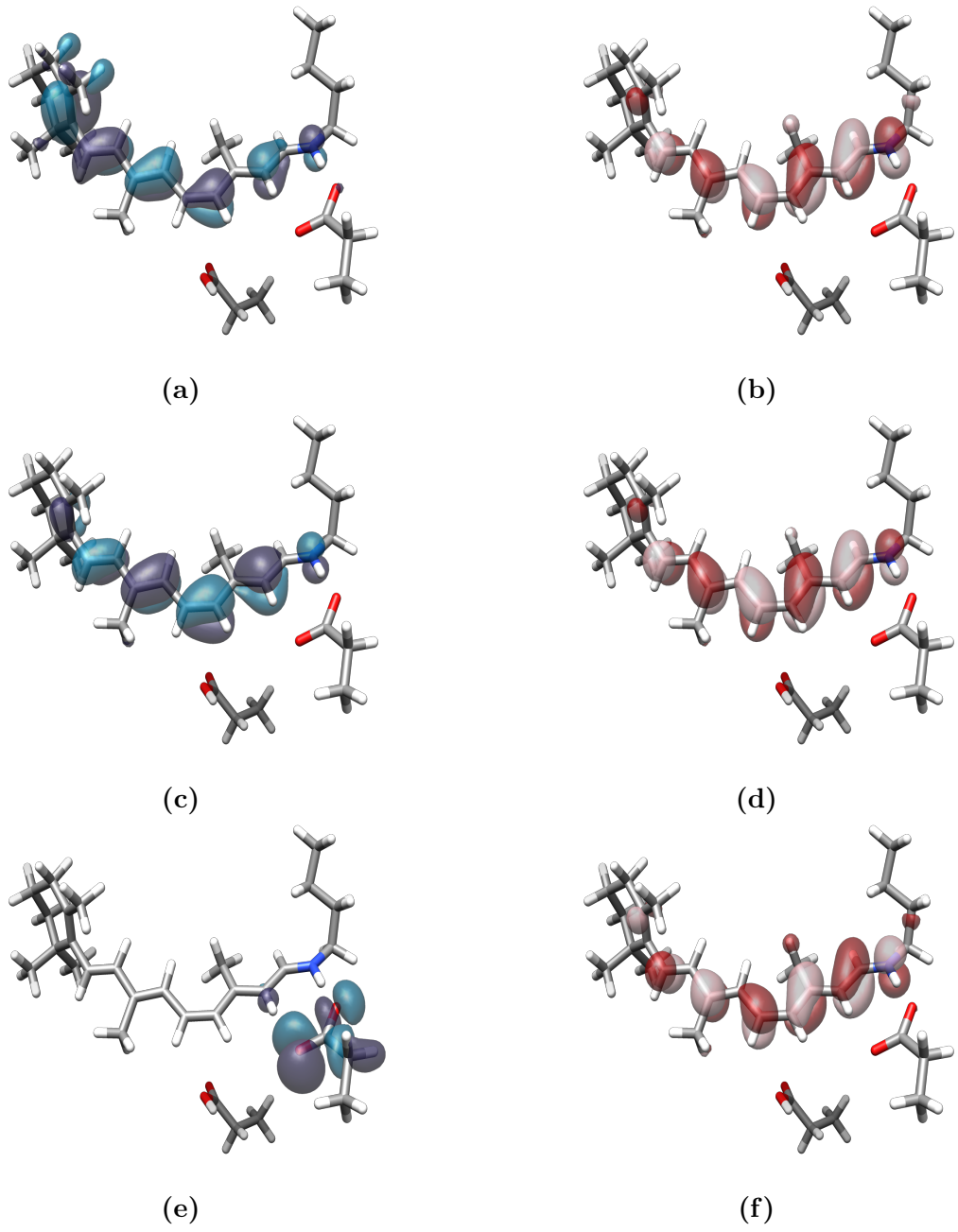

Figure 4.14: Stick representation of the SBHcarb(0) molecular model of rhodopsin. Natural transition orbitals are plotted with a contour value of 0.03 a.u. (a) and (b) Fourth excitation of occupied and virtual NTO (DFT) of SBHcarb(0) (c) and (d) First excitation of occupied and virtual NTO (CCS) of SBHcarb(0) (e) and (f) First improper excitation of occupied and virtual NTO (DFT) of SBHcarb(0).

The same explanation holds true for SBHcarb(0)imidwaters that we could not find the relevant excitation earlier than number 16 for DFT based excitation and plots since in addition to Glu-113, we have imidazole overlapping problem too. And finally, in the worst case, SBHcarb(-)imidwaters, that we have three overlapping interference, and we couldn't find the relevant excitation even after plotting 20 NTOs. However, for both of them, the CCS generated NTOs related to first excitation was the relevant excitation

Rhodopsin models	RICC2 [eV]	f	DFT [eV]	f
SBcarb(-)	1.537	0.000	2.828	1.564
SBcarb(0)	3.380	1.704	2.800	1.433
SBcarb(0)imdidwaters	3.366	–	2.801	1.485
SBcarb(-)imdidwaters	0.648	–	2.830	1.448
SBHcarb(-)	2.738	0.000	2.616	1.293
SBHcarb(0)	2.649	0.015	2.554	1.189
SBHcarb(0)imdidwaters	2.856	–	2.646	1.122
SBHcarb(-)imdidwaters	0.717	–	–	–

Table 4.8: Selected relevant lowest excitation energies and associated oscillator strengths (f) of rhodopsin Glu-113 and Glu-181 different protonation states calculated at RICC2/cc-pVDZ and DFT/B3LYP level of theory.

to the photoisomerization process. All selected relevant lowest excitation energies of above-discussed cluster models of rhodopsin are listed in table 4.8. For complete table of excitation energies please refer to table A2.1 and table A2.2 in the appendix. We previously mentioned an important controversy over the protonation states of Glu-181 in rhodopsin [18, 19]. Frähmcke et al.[18] by the means of QM/MM calculations postulates that although spectroscopic studies are not significantly in favor of any specific protonation state of Glu-181, but they results are slightly in favor of negatively charged Glu-181. On the other side, we have studies concluded conversely about Glu-181 [50]. For instance, Yan et al.[56] via Raman Spectroscopy techniques proposed that Glu-181 is uncharged in the dark state and in metarhodopsin-I state, we observe a counterion switch from Glu-113 to Glu-181 which means the Glu-181 proton moves through hydrogen bond network to Glu-113. However, it seems that Glu-181 protonation state has not entirely cleared of controversy.

As we mentioned, our results indicates clearly that protonated state of Glu-181 doesn't have any interfering orbital overlap with conjugated π orbitals of retinal polyene. This means that, as we saw for SBcarb(0), we have the lowest excitation, with a dominant oscillator strength, as the most relevant excitation. Which is in accordance, with other studies indicating that photoexcitation process in rhodopsin has been tailored such that the most probable and suitable excitation has the one dominant oscillator strength. This phenomenon maximize the quantum yield of the process [27, 43].

A question may arise here that if we have this interfering effect of the negatively charged Glu-181 and its counterpart in blue cone that blueshifts the relevant excitation with a dominant oscillator strength, why we cannot see it in other related studies?

One answer might be that they haven't included it in their molecular models. For instance, In a study, Send et al. have used reduced-virtual-space (RVS) approach within RICC2/def2-TZVP level of theory to calculate lowest excitation energy of a rhodopsin

cluster model consisting of 165 atoms. In RVS approach, virtual orbital with energies higher than a pre-defined value will be removed from CC2 calculation. They used 1KPN blue cone homology model to construct their model, but the chromophore is protonated from of retinal *Schiff* [47] base (SBH), and the residues that they listed are inconsistent with what we observed from 1KPN homology model. They didn't include Glu-181 or more precisely Glu-178, thus, they haven't experienced the unexpected energy shift in excitation energy. However, they reported the lowest excitation energy of their model as 2.92 eV which is close to our SGHW cluster model excitation energy which was calculated at RICC2/cc-pVDZ level through CorNFLEx scheme. Our SGHW is not an identical model, but is the closest among our cluster models to the model that they have defined.

In another study, the excitation enregy for bacteriorhodopsin at the SORCI-DFTB/MM level of theory is calculated as 2.34 eV [55]. In bacteriorhodopsin, we have protonated retinal *Schiff* base but with opposite photoisomerization: all–trans to the 13–cis isomer. It seems that aspartic acid is the counterion, and there is no other carboxylate group near the chromophore to interfere the excitation energies [54].

And similarly, in a study, TDDFT/B3LYP in combination with reduction of virtual space (RVS) approximation was applied on a full quantum mechanically described clusters of rhodopsin and blue cone. They calculate 2.81 eV and 2.53 eV as excitation energies for blue cone and rhodopsin respectively. In their models they used another crystal structure (1HZX) which it doesn't have Glu-181. However, they included Glu-122 in its protonated form and not included His-211, and it might be a good reason for why they haven't experienced Glu-181 and His-211 energy shifts observation [27].

Another reason might be related to this fact that in some study they used embedded charges instead of surrounded residues, and not include them in their active orbital space [60].

And final scenario is related to the fact that in rhodopsin, excitation energy is highly dependent on ground-state optimization technique [55]. The structural optimization specifically become more important when we have resonance structure with conjugated π orbitals in the vicinity of the chromophore. Then the orientation of the orbitals in space significantly affects the overlap integrals and consequently the resulted excitation energies. Since we allowed carboxylic group to be optimized with our optimization method, it might have affected our resulted excitation energies.

4.6 Cluster models' excitation energies overview

It is now a good time to a have an overview of the obtained results. starting from the rhodopsin cluster models, we have used information in table 4.4 to simulate UV/Visible

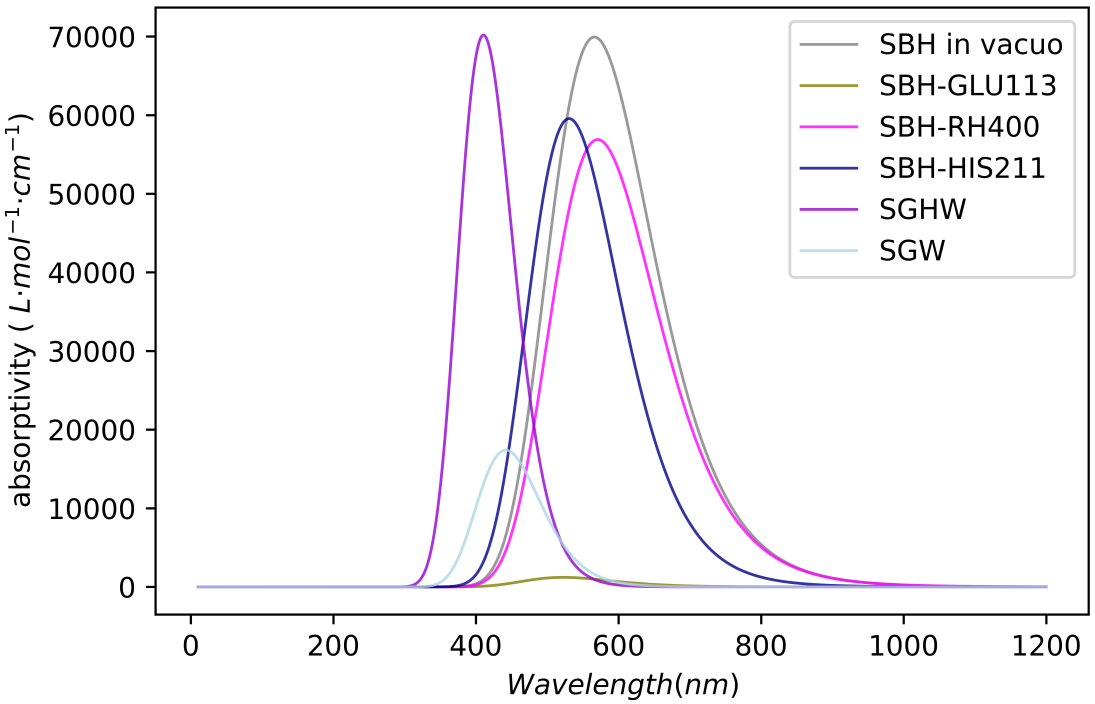

Figure 4.15: Gaussian broadening RICC2/cc-pVDZ lowest excitation energies of rhodopsin cluster models using 0.4 eV as standard deviation.

absorption spectrum of rhodopsin cluster models, based on the lowest excitation energy obtained at RICC2/cc-pVDZ level and associated oscillator strength, exploiting Gaussian broadening function and using 0.4 eV as standard deviation of the Gaussian function [1]. As we can see in figure 4.15, SBH *in vacuo* has a peak with high intensity at around 566 nm. As we mentioned in section 4.3, the introduction of Glu-113, His-211, and water molecules and also steric effect of the protein results in blueshifting in absorption spectrum. The highest effect with highest oscillator strength is related to SGHW cluster model. Notice that including Glu-113 at first step (SBH-GLU113) resulted in blueshifting with a very low oscillator strength. However, after inclusion of His-211 (SGHW), we can see the oscillator strength of the cluster model has been improved.

Moving to blue cone cluster models, we again have plotted (figure 4.16) UV/Visible absorption spectrum with Gaussian broadening function and using 0.4 eV as standard deviation of the Gaussian function. By comparing SB *in vacuo* and SB-BL400 models, we can see a redshifting effect. Comparing SG and SGT with SB-BL400, we notice a converging of excitation energies toward experimental value. Surprisingly, SB-BL400 excitation energy at DFT/B3LYP level is very close to experimental absorption value of the blue cone. The relatively large deviation of BL400 cluster models absorption spectrum comparing with experimental value might be related to removing lots of apparently

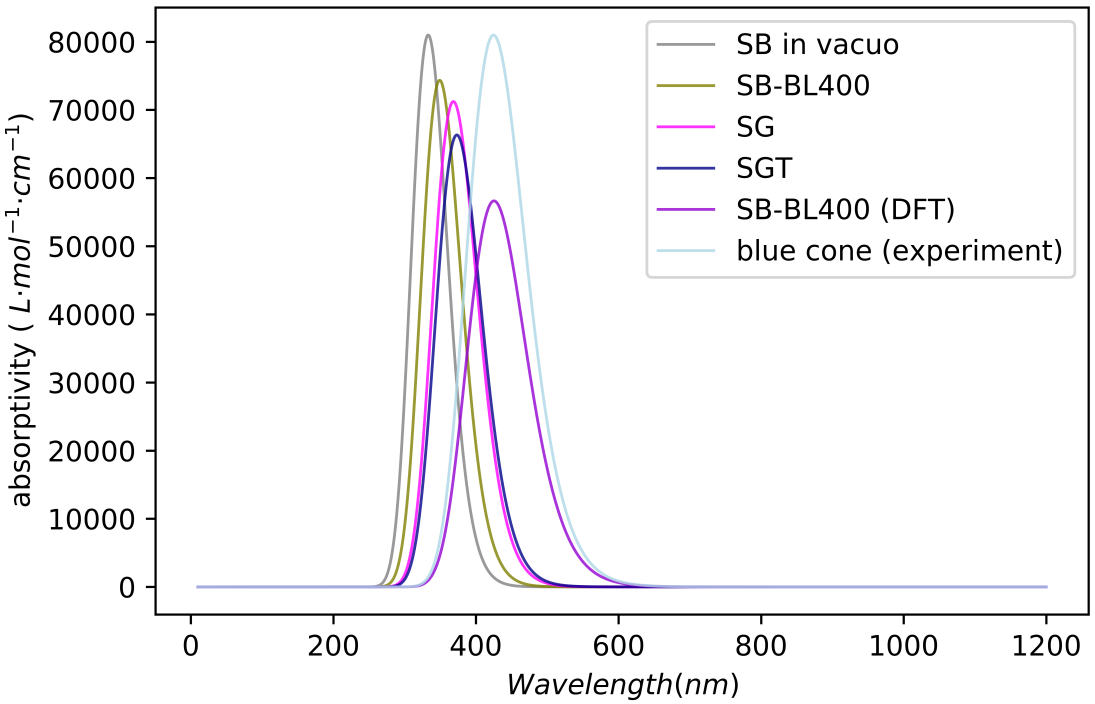

Figure 4.16: Gaussian broadening RICC2/cc-pVDZ lowest excitation energies of blue cone cluster models using 0.4 eV as standard deviation.

important residues, such as residues participating in hydrogen bonding network of the blue cone. However, since even our isolated SB-BL400 and *in vacuo* structure excitation energies deviates significantly from other studies (table 4.3), then the error might be related to our quantum chemical method or the optimized structure that we used.

4.7 Why RSB is as SB in blue cone and as SBH in rhodopsin?

To address this question, it might be better to rephrase it into a more clear and feasible question: what is the pKa of *Schiff* base in rhodopsin and blue cone protein environment? Interestingly, pKa of *Schiff* base is an important question not only to understand the protonation states of RSB in rhodopsin and blue cone, but to understand the photoactivation of RSB and mechanism of visual cycle. Inspecting the visual cycle in rod photoreceptor cells, we see that during dark state and metarhodopsin-I, the RSB is in its protonated form. And, during metarhodopsin-II state, *Schiff* base gains a higher pKa value and become deprotonted in higher proportion of RSB molecules [61].

Zhu et al. has shown that we can define that pKa value of the *Schiff* base as a function of C5=C6-C7=C8 dihedral angle which is determining the spacial position of β-ionine

ring with respect to polyene. It seems that in dark state we have a planar conformation of RSB and during activation, the protein pocket allows the β-ionine ring to rotate and from a non-planar conformation elicit a higher pKa.

At first attempt, we used above information to calculate the pKa differences in rhodopsin and blue cone. We measured the C5=C6-C7=C8 dihedral angle for RSB in rhodopsin and blue cone which turns to be -49.7° and -50.5° respectively. Plugging these numbers into Zhu et al. resulted function, both pKa will be almost 7.25.

This result indicates that we should relate the possible difference of pKa between rhodopsin and blue cone to the different protein environment that each of them lies.

To consider this, we use fundamental thermodynamics relation

$$pK_a = \frac{\Delta G_a}{2.303RT} \tag{4.1}$$

and thermodynamic cycle [12]

$$\Delta G_a = \Delta G_g - \Delta G_{sol}^{AH} + \Delta G_{sol}^{A^-} + \Delta G_{sol}^{H^+} \tag{4.2}$$

And considering the fact that above thermodynamic cycle can be simplified to

$$\Delta G_a = \Delta G_{protein}^{A^-} - \Delta G_{protein}^{AH} \tag{4.3}$$

Since in our protein-ligand model, we just need to consider free energy that is consumed to move a proton from the *Schiff* base and putting it on the carboxylate group.

We can do another simplification by considering the fact that RSB is almost fixed in place with high activation barriers against thermal conformational changes [61] and assuming that protonated and deprotonated states have the same vibrational partition function, then we can say $G^{A^-} \approx E^{A^-}$ and $G^{AH} \approx E^{AH}$.

Thus, to calculate pKa we calculate the electronic energy of E^{A^-} and E^{AH} , that in our model are SB and SBH respectively (in the full protein environment of RH400 and BL400), at DFT/B3LYP level. Plugging into equation 4.3 and 4.1, the *Schiff* base pKa values are -195.52 for blue cone model and 22.58 for rhodopsin model. The enormous different values clearly shows that RSB is almost always in its deprotonated form (SB) in blue cone and porotonated form (SBH) in rhodopsin. To compare these values with pKa of RSB in water, we used Schrödinger Release 2019-4, Jaguar [57, 29] software to calculate to calculate pKa as 15.5. Comparing this value with our calculated values, we can notice the huge impact of protein environment on the protonation states of RSB, and to what extent this protonation state is important for visual cycle and GPCRs performance.

5 Conclusion

The effect of protein environment on absorption spectrum of retinal *Schiff* base have been studied at RICC2/cc-pVDZ and DFT/B3LYP level of theory in rhodopsin and blue cone which are responsible for dim light (scotopic) and color vision respectively [25]. Experiments show rhodopsin absorbs at 498 nm (2.49 eV) [45, 42]. RICC2 excitation energies show porotonated retinal *Schiff* base (SBH), which is the most prevalent form inside the rhodopsin, absorbs at 571 nm (2.17 eV), and our value was close to other studies and its experimental value, 2.03 eV (table 4.3). Comparing this value with the SBH excitation energies in gas phase (2.19 eV), we conclude that steric effect of rhodopsin on spectral tuning of SBH is negligible. An interesting observation took place, when we added Glu-113 to SBH (figure 3.1), and we calculate an excitation energy (2.37 eV) close to rhodopsin absorption. We also added other residues and two water molecules which resulted in blueshifting the absorption spectrum (table 4.4). Our results confirms the reportedly postulated claim that Glu-113 as the counterion of the *Shiff* base affords considerable share of 0.46 eV rhodopsin shift. However, we add this fact that SBH-GLU113 cluster model has a poor oscillator strength and this problem significantly improved by other residues, more specifically His-211 (figure 4.15).

The situation in blue cone is a little bit different. Blue cone absorbs at 425 nm (2.92 eV), and our RICC2 excitation energies deviates largely from this value; however, slightly converging to experimental value (table 4.5). On the other hand, our DFT values are much closer to experimental value, especially our SB-BL400 model excitation energy (2.92 eV) which is identical to it. The oscillator strength for all cluster models are dominantly large. Another important observation is related to protonation states of Glu-181 and Glu-178 in rhodopsin and blue cone respectively. In both cases, we conclude that protonated form of these residues leads to a more efficient photoisomerization with higher quantum yield. Meaning that the proper excitation, which leads to photoisomerization, is the excitation with lowest excitation energy and dominant oscillator strength. This observation, also reveals structural optimization of the ground state is quite important due to long conjugated π orbital of RSB which make the space very sensitive to considerable orbital overlaps. Finally, we conclude that proton affinity of the *Schiff* base is much larger in rhodopsin than in blue cone by calculating their pKas.

6 Further work

During this study, and also form other studies, we clearly noticed the ground-state dependency of excitation energies of visual pigments. In such a case, molecular dynamics methods can help us to have a better description of ground and excited states in terms of a more comprehensive potential energy surface. Considering the computational cost of *ab initio* quantum chemical methods, we chose our methods which clearly was not sufficient to include all important residues of visual pigments in the cluster models. In this regard, a more complete cluster model, treated with a higher level *ab initio* method, with a more complete basis set may reduce the possible errors significantly.

References

[1] Creating uv/visible plots from the results of excited states calculations. https://gaussian.com/uvvisplot/. Accessed: 2020-01-10.

[2] Lsdalton-2018 electronic structure program documentation. https://daltonprogram.org/documentation/. Accessed: 2020-01-10.

[3] Nwchem: high performance computational software documentation. http://www.nwchem-sw.org/index.php/Release66:NWChem_Documentation. Accessed: 2020-01-10.

[4] Schrödinger release 2019-4: Jaguar pka related article. https://www.schrodinger.com/science-articles/role-conformations-dft-based-pka-prediction. Accessed: 2020-01-10.

[5] Stallo cluster. https://hpc-uit.readthedocs.io/en/latest/stallo/stallo.html. Accessed: 2020-01-10.

[6] Aidas, K., Angeli, C., Bak, K. L., Bakken, V., Bast, R., Boman, L., Christiansen, O., Cimiraglia, R., Coriani, S., Dahle, P., Dalskov, E. K., Ekström, U., Enevoldsen, T., Eriksen, J. J., Ettenhuber, P., Fernández, B., Ferrighi, L., Fliegl, H., Frediani, L., Hald, K., Halkier, A., Hättig, C., Heiberg, H., Helgaker, T., Hennum, A. C., Hettema, H., Hjertenæs, E., Høst, S., Høyvik, I.-M., Iozzi, M. F., Jansík, B., Jensen, H. J. Aa., Jonsson, D., Jørgensen, P., Kauczor, J., Kirpekar, S., Kjærgaard, T., Klopper, W., Knecht, S., Kobayashi, R., Koch, H., Kongsted, J., Krapp, A., Kristensen, K., Ligabue, A., Lutnæs, O. B., Melo, J. I., Mikkelsen, K. V., Myhre, R. H., Neiss, C., Nielsen, C. B., Norman, P., Olsen, J., Olsen, J. M. H., Osted, A., Packer, M. J., Pawlowski, F., Pedersen, T. B., Provasi, P. F., Reine, S., Rinkevicius, Z., Ruden, T. A., Ruud, K., Rybkin, V. V., Sałek, P., Samson, C. C. M., de Merás, A. S., Saue, T., Sauer, S. P. A., Schimmelpfennig, B., Sneskov, K., Steindal, A. H., Sylvester-Hvid, K. O., Taylor, P. R., Teale, A. M., Tellgren, E. I., Tew, D. P., Thorvaldsen, A. J., Thøgersen, L., Vahtras, O., Watson, M. A., Wilson, D. J. D., Ziolkowski, M., and Ågren, H. (2014). The Dalton quantum chemistry program system. *WIREs Comput. Mol. Sci.*, 4(3):269–284.

[7] Altun, A., Yokoyama, S., and Morokuma, K. (2008). Mechanism of spectral tuning going from retinal in vacuo to bovine rhodopsin and its mutants: Multireference ab initio quantum mechanics/molecular mechanics studies. *The Journal of Physical Chemistry B*, 112(51):16883–16890.

[8] Andruniów, T., Ferré, N., and Olivucci, M. (2004). Structure, initial excited-state relaxation, and energy storage of rhodopsin resolved at the multiconfigurational perturbation theory level. *Proceedings of the National Academy of Sciences*, 101(52):17908–17913.

[9] Atkins, P. W. and Atkins, P. W. (2010). *Molecular quantum mechanics*. Oxford University Press.

[10] Baudin, P., Kjærgaard, T., and Kristensen, K. (2017). Cc2 oscillator strengths within the local framework for calculating excitation energies (lofex). *The Journal of Chemical Physics*, 146(14):144107.

[11] Baudin, P. and Kristensen, K. (2017). Correlated natural transition orbital framework for low-scaling excitation energy calculations (cornflex). *The Journal of Chemical Physics*, 146(21):214114.

[12] Bochevarov, A. D., Watson, M. A., Greenwood, J. R., and Philipp, D. M. (2016). Multiconformation, density functional theory-based pka prediction in application to large, flexible organic molecules with diverse functional groups. *Journal of Chemical Theory and Computation*, 12(12):6001–6019. PMID: 27951674.

[13] Boys, S. F. and Egerton, A. C. (1950). Electronic wave functions - i. a general method of calculation for the stationary states of any molecular system. *Proceedings of the Royal Society of London. Series A. Mathematical and Physical Sciences*, 200(1063):542–554.

[14] Bravaya, K., Bochenkova, A., Granovsky, A., and Nemukhin, A. (2007). An opsin shift in rhodopsin: retinal s0s1 excitation in protein, in solution, and in the gas phase. *Journal of the American Chemical Society*, 129(43):13035–13042. PMID: 17924622.

[15] Christiansen, O. (2006). Coupled cluster theory with emphasis on selected new developments. *Theoretical Chemistry Accounts*, 116(1):106–123.

[16] Christiansen, O., Koch, H., and Jørgensen, P. (1995). The second-order approximate coupled cluster singles and doubles model cc2. *Chemical Physics Letters*, 243(5):409 – 418.

[17] Dennis, J. and Moré, J. (1977). Quasi-Newton Methods, Motivation and Theory. *SIAM Review*, 19(1):46–89.

[18] Frähmcke, J. S., Wanko, M., Phatak, P., Mroginski, M. A., and Elstner, M. (2010). The protonation state of glu181 in rhodopsin revisited: Interpretation of experimental data on the basis of qm/mm calculations. *The Journal of Physical Chemistry B*, 114(34):11338–11352. PMID: 20698519.

[19] Hall, K. F., Vreven, T., Frisch, M. J., and Bearpark, M. J. (2008). Three-layer oniom studies of the dark state of rhodopsin: The protonation state of glu181. *Journal of Molecular Biology*, 383(1):106 – 121.

[20] Harrison, N. (2003). An introduction to density functional theory. *Nato Science Series Sub Series III Computer and Systems Sciences*, 187:45–70.

[21] Helgaker, T., Jørgensen, P., and Olsen, J. (2000). *Molecular electronic-structure theory*. John Wiley Sons.

[22] Hohenberg, P. and Kohn, W. (1964). Inhomogeneous electron gas. *Phys. Rev.*, 136:B864–B871.

[23] Hättig, C. (2006). *Beyond Hartree-Fock: MP2 and coupled-cluster methods for large systems*. Computational Nanoscience: Do It Yourself!, J. Grotendorst, S. Blügel, D. Marx (Eds.), John von Neumann Institute for Computing, Jülich, NIC Series.

[24] Høyvik, I.-M., Myhre, R. H., and Koch, H. (2017). Correlated natural transition orbitals for core excitation energies in multilevel coupled cluster models. *The Journal of Chemical Physics*, 146(14):144109.

[25] Imamoto, Y. and Shichida, Y. (2014). Cone visual pigments. *Biochimica et Biophysica Acta (BBA) - Bioenergetics*, 1837(5):664 – 673. Retinal Proteins.

[26] Janz, J. M. and Farrens, D. L. (2004). Role of the retinal hydrogen bond network in rhodopsin schiff base stability and hydrolysis. *The Journal of Biological Chemistry*, 279(53):55886 – 55894.

[27] Kaila, V. R. I., Send, R., and Sundholm, D. (2012). The effect of protein environment on photoexcitation properties of retinal. *The Journal of Physical Chemistry B*, 116(7):2249–2258. PMID: 22166007.

[28] Kakitani, H., Kakitani, T., Rodman, H., and Honig, B. (1985). On the mechanism of wavelength regulation in visual pigments. *Photochemistry and Photobiology*, 41(4):471–479.

[29] Klicić, J. J., Friesner, R. A., Liu, S.-Y., and Guida, W. C. (2002). Accurate prediction of acidity constants in aqueous solution via density functional theory and self-consistent reaction field methods. *The Journal of Physical Chemistry A*, 106(7):1327–1335.

[30] Koch, H. and Jo/rgensen, P. (1990). Coupled cluster response functions. *The Journal of Chemical Physics*, 93(5):3333–3344.

[31] Kropf, A. and Hubbard, R. (1958). The mechanism of bleaching rhodopsin. *Annals of the New York Academy of Sciences*, 74(2):266–280.

[32] Kurth, S., Marques, M., and Gross, E. (2003). Electronic structure: Density functional theory.

[33] McHale, J. L. (1999). *Molecular spectroscopy*. Prentice-Hall.

[34] McWeeny, R. (1950). Gaussian approximations, to wave functions. *Nature*, 166:21–22.

[35] Montero, L. A., Díaz, L. A., and Bader, R. (2003). *Introduction to advanced topics in computational chemsitry*. Facultad de Química, Universidad de La Habana, La Habana 10400, Cuba.

[36] Neitz, M., Neitz, J., and Jacobs, G. (1991). Spectral tuning of pigments underlying red-green color vision. *Science*, 252(5008):971–974.

[37] Nouredine, Z. (2009). *Quantum mechanics: concepts and applications*. John Wiley Sons.

[38] Okada, T., Sugihara, M., Bondar, A.-N., Elstner, M., Entel, P., and Buss, V. (2004). The retinal conformation and its environment in rhodopsin in light of a new 2.2Å crystal structure††this paper is dedicated to dr yoshimasa kyogoku. *Journal of Molecular Biology*, 342(2):571 – 583.

[39] Palczewski, K. (2006). G protein–coupled receptor rhodopsin. *Annual Review of Biochemistry*, 75(1):743–767. PMID: 16756510.

[40] Patel, A. B., Crocker, E., Reeves, P. J., Getmanova, E. V., Eilers, M., Khorana, H. G., and Smith, S. O. (2005). Changes in interhelical hydrogen bonding upon rhodopsin activation. *Journal of Molecular Biology*, 347(4):803 – 812.

[41] Pettersen, E. F., Goddard, T. D., Huang, C. C., Couch, G. S., Greenblatt, D. M., Meng, E. C., and Ferrin, T. E. (2004). Ucsf chimera—a visualization system for exploratory research and analysis. *Journal of Computational Chemistry*, 25(13):1605–1612.

[42] Sakmar, T. P., Menon, S. T., Marin, E. P., and Awad, E. S. (2002). Rhodopsin: Insights from recent structural studies. *Annual Review of Biophysics and Biomolecular Structure*, 31(1):443–484. PMID: 11988478.

[43] Schreiber, M. and Buss, V. (2003). Origin of the bathochromic shift in the early photointermediates of the rhodopsin visual cycle: A casscf/caspt2 study. *International Journal of Quantum Chemistry*, 95(6):882–889.

[44] Schreiber, M., Buß, V., and Sugihara, M. (2003). Exploring the opsin shift with ab initio methods: Geometry and counterion effects on the electronic spectrum of retinal. *The Journal of Chemical Physics*, 119(23):12045–12048.

[45] Sekharan, S., Sugihara, M., and Buss, V. (2007). Origin of spectral tuning in rhodopsin—it is not the binding pocket. *Angewandte Chemie International Edition*, 46(1-2):269–271.

[46] Send, R., Kaila, V. R. I., and Sundholm, D. (2011a). Benchmarking the approximate second-order coupled-cluster method on biochromophores. *Journal of Chemical Theory and Computation*, 7(8):2473–2484. PMID: 26606621.

[47] Send, R., Kaila, V. R. I., and Sundholm, D. (2011b). Reduction of the virtual space for coupled-cluster excitation energies of large molecules and embedded systems. *The Journal of Chemical Physics*, 134(21):214114.

[48] Slater, J. C. (1930). Atomic shielding constants. *Phys. Rev.*, 36:57–64.

[49] Stenkamp, R., Filipek, S., Driessen, C., Teller, D., and Palczewski, K. (2002). Crystal structure of rhodopsin: a template for cone visual pigments and other g protein-coupled receptors. *Biochimica et Biophysica Acta (BBA) - Biomembranes*, 1565(2):168 – 182. Membrane Protein Structure.

[50] Sugihara, M., Buss, V., Entel, P., Hafner, J., Bondar, A., Elstner, M., and Frauenheim, T. (2004). Ab initio, tight-binding and qm/mm calculations of the rhodopsin chromophore in its binding pocket. *Phase Transitions*, 77(1-2):31–45.

[51] Szabo, A. and Ostlund, N. S. (1996). *Modern quantum chemistry: introduction to advanced electronic structure theory*. Dover Publications.

[52] Sæther, S. (2017). Reduced orbital space coupled-cluster calculations using a multilevel hartree-fock wave function. Master's thesis, Norwegian University of Science and Technology, Høgskoleringen 1, 7491 Trondheim, Norway.

[53] Valiev, M., Bylaska, E., Govind, N., Kowalski, K., Straatsma, T., Dam, H. V., Wang, D., Nieplocha, J., Apra, E., Windus, T., and de Jong, W. (2010). Nwchem: A comprehensive and scalable open-source solution for large scale molecular simulations. *Computer Physics Communications*, 181(9):1477 – 1489.

[54] Vreven, T. and Morokuma, K. (2003). Investigation of the s0 to s1 excitation in bacteriorhodopsin with the oniom(mo:mm) hybrid method. *Theoretical chemistry accounts*, 109:125–132.

[55] Wanko, M., Hoffmann, M., Strodel, P., Koslowski, A., Thiel, W., Neese, F., Frauenheim, T., and Elstner, M. (2005). Calculating absorption shifts for retinal proteins: computational challenges. *The Journal of Physical Chemistry B*, 109(8):3606–3615. PMID: 16851399.

[56] Yan, E. C. Y., Kazmi, M. A., Ganim, Z., Hou, J.-M., Pan, D., Chang, B. S. W., Sakmar, T. P., and Mathies, R. A. (2003). Retinal counterion switch in

the photoactivation of the g protein-coupled receptor rhodopsin. *Proceedings of the National Academy of Sciences*, 100(16):9262–9267.

[57] Yu, H. S., Watson, M. A., and Bochevarov, A. D. (2018). Weighted averaging scheme and local atomic descriptor for pka prediction based on density functional theory. *Journal of Chemical Information and Modeling*, 58(2):271–286. PMID: 29356524.

[58] Zener, C. (1930). Analytic atomic wave functions. *Phys. Rev.*, 36:51–56.

[59] Zhou, H.-X. and Pang, X. (2018). Electrostatic interactions in protein structure, folding, binding, and condensation. *Chemical Reviews*, 118(4):1691–1741. PMID: 29319301.

[60] Zhou, X., Sundholm, D., Wesołowski, T. A., and Kaila, V. R. I. (2014). Spectral tuning of rhodopsin and visual cone pigments. *Journal of the American Chemical Society*, 136(7):2723–2726. PMID: 24422511.

[61] Zhu, S., Brown, M. F., and Feller, S. E. (2013). Retinal conformation governs pka of protonated schiff base in rhodopsin activation. *Journal of the American Chemical Society*, 135(25):9391–9398. PMID: 23701524.

Appendix

A1 Blue cone higher excitation energies

Excitation energies related to blue cone: SBcarb(-)										
	1st	2nd	3rd	4th	5th	6th	7th	8th	9th	10th
DFT [eV]	0.292	0.460	1.437	1.688	1.973	2.546	2.827	2.863	3.113	3.211
f	0.000	0.000	0.031	0.000	0.000	0.011	0.003	1.482	0.000	0.000
RICC2 [eV]	1.391	1.638	2.093	2.970	3.213	3.459	3.660	4.433	4.597	4.787
f	0.000	0.000	0.000	0.000	0.000	1.894	0.000	0.113	0.011	0.214
Excitation energies related to blue cone: SBcarb(0)										
	1st	2nd	3rd	4th	5th	6th	7th	8th	9th	10th
DFT [eV]	2.815	3.526	3.579	3.931	4.059	4.576	4.592	4.693	4.870	4.967
f	1.326	0.220	0.158	0.057	0.005	0.000	0.148	0.014	0.045	0.016
RICC2 [eV]	3.416	4.422	4.497	4.670	5.352	–	–	–	–	–
f	1.772	0.265	0.018	0.144	0.136	–	–	–	–	–
Excitation energies related to blue cone: SBHcarb(-)										
	1st	2nd	3rd	4th	5th	6th	7th	8th	9th	10th
DFT [eV]	0.366	0.461	1.147	1.513	1.541	1.603	1.859	2.136	2.621	2.714
f	0.000	0.000	0.023	0.016	0.075	0.001	0.000	0.000	0.452	0.602
RICC2 [eV]	0.568	0.899	1.288	2.142	2.316	2.466	2.643	2.804	3.023	3.095
f	0.000	0.000	0.000	0.029	0.000	0.106	0.000	0.002	0.000	1.476
Excitation energies related to blue cone: SBHcarb(0)										
	1st	2nd	3rd	4th	5th	6th	7th	8th	9th	10th
DFT [eV]	0.888	1.273	1.323	2.424	2.577	2.855	3.021	3.354	3.822	3.877
f	0.020	0.087	0.000	0.184	0.755	0.052	0.000	0.498	0.172	0.000
RICC2 [eV]	1.853	2.206	2.559	2.972	4.136	–	–	–	–	–
f	0.027	0.093	0.000	1.383	0.218	–	–	–	–	–

Table A1.1: Higher excitation energies and associated oscillator strengths (f) of blue cone Glu-110 and Glu-178 different protonation states calculated at RICC2/cc-pVDZ and DFT/B3LYP level of theory.

A2 Rhodopsin higher excitation energies

Excitation energies related to rhodopsin: SBcarb(-)										
	1st	2nd	3rd	4th	5th	6th	7th	8th	9th	10th
DFT [eV]	0.237	0.459	1.530	1.751	2.056	2.374	2.544	2.611	2.782	2.828
f	0.000	0.000	0.019	0.000	0.000	0.000	0.017	0.000	0.000	1.564
RICC2 [eV]	1.537	1.762	2.232	3.417	3.633	–	–	–	–	–
f	0.000	0.000	0.000	1.886	0.138	–	–	–	–	–
Excitation energies related to rhodopsin: SBcarb(0)										
	1st	2nd	3rd	4th	5th	6th	7th	8th	9th	10th
DFT [eV]	2.800	2.977	3.479	3.945	4.424	4.550	4.636	4.663	4.882	4.900
f	1.433	0.058	0.235	0.075	0.003	0.170	0.041	0.000	0.000	0.020
RICC2 [eV]	3.380	3.539	4.292	4.698	5.300	–	–	–	–	–
f	1.704	0.208	0.185	0.143	0.194	–	–	–	–	–
Excitation energies related to rhodopsin: SBcarb(0)imidwaters										
	1st	2nd	3rd	4th	5th	6th	7th	8th	9th	10th
DFT [eV]	0.721	1.773	1.934	2.057	2.321	2.337	2.596	2.607	2.771	2.801
f	0.000	0.000	0.000	0.000	0.000	0.000	0.000	0.000	0.000	1.486
RICC2 [eV]	3.366	3.569	3.776	4.279	4.738	–	–	–	–	–
f	–	–	–	–	–	–	–	–	–	–
Excitation energies related to rhodopsin: SBcarb(-)imidwaters										
	1st	2nd	3rd	4th	5th	6th	7th	8th	9th	10th
DFT [eV]	0.496	0.559	0.925	1.224	1.383	1.549	1.621	1.851	1.879	2.119
f	0.000	0.000	0.000	0.000	0.000	0.000	0.000	0.000	0.000	0.000
	11th	12th	13th	14th	15th	16th	17th	18th	19th	20th
DFT [eV]	2.139	2.153	2.199	2.255	2.275	2.326	2.467	2.631	2.829	2.864
f	0.002	0.000	0.000	0.000	0.000	0.000	0.000	0.000	1.449	0.000
	1st	2nd	3rd	4th	5th	6th	7th	8th	9th	10th
RICC2 [eV]	0.648	1.146	1.494	1.945	2.359	–	–	–	–	–
f	–	–	–	–	–	–	–	–	–	–

Table A2.1: Higher excitation energies and associated oscillator strengths (f) of rhodopsin (SB) Glu-113 different protonation states calculated at RICC2/cc-pVDZ and DFT/B3LYP level of theory.

Excitation energies related to rhodopsin: SBHcarb(-)										
	1st	2nd	3rd	4th	5th	6th	7th	8th	9th	10th
DFT [eV]	0.348	0.463	1.586	1.603	1.931	2.076	2.157	2.213	2.616	2.832
f	0.000	0.000	0.000	0.018	0.000	0.026	0.046	0.000	1.293	0.087
RICC2 [eV]	0.577	0.917	1.299	2.399	2.738	2.763	2.904	3.044	3.110	3.421
f	0.000	0.000	0.000	0.000	0.000	0.002	1.479	0.219	0.000	0.006
Excitation energies related to rhodopsin: SBHcarb(0)										
	1st	2nd	3rd	4th	5th	6th	7th	8th	9th	10th
DFT [eV]	1.302	1.831	1.894	2.554	2.998	3.334	3.519	3.582	3.796	3.942
f	0.000	0.022	0.029	1.189	0.001	0.467	0.011	0.003	0.087	0.000
RICC2 [eV]	2.649	2.867	2.969	3.308	4.114	–	–	–	–	–
f	0.015	0.980	0.635	0.006	0.302	–	–	–	–	–
Excitation energies related to rhodopsin: SBHcarb(0)imidwaters										
	1st	2nd	3rd	4th	5th	6th	7th	8th	9th	10th
DFT [eV]	0.588	1.078	1.167	1.290	1.466	1.675	1.908	2.004	2.150	2.185
f	0.000	0.000	0.000	0.000	0.000	0.000	0.000	0.014	0.037	0.000
	11th	12th	13th	14th	15th	16th	17th	18th	19th	20th
DFT [eV]	2.385	2.424	2.485	2.609	2.639	2.646	2.655	2.914	2.941	2.997
f	0.000	0.000	0.000	0.000	0.200	1.122	0.000	0.000	0.000	0.000
	1st	2nd	3rd	4th	5th	6th	7th	8th	9th	10th
RICC2 [eV]	2.856	3.027	3.117	3.548	4.111	–	–	–	–	–
f	–	–	–	–	–	–	–	–	–	–
Excitation energies related to rhodopsin: SBHcarb(-)imidwaters										
	1st	2nd	3rd	4th	5th	6th	7th	8th	9th	10th
DFT [eV]	0.353	0.549	0.836	1.040	1.202	1.231	1.342	1.572	1.584	1.585
f	0.001	0.000	0.000	0.000	0.000	0.000	0.000	0.000	0.000	0.000
	11th	12th	13th	14th	15th	16th	17th	18th	19th	20th
DFT [eV]	1.685	1.725	1.745	1.752	2.100	2.110	2.262	2.283	2.328	2.346
f	0.000	0.000	0.000	0.000	0.000	0.000	0.011	0.000	0.000	0.000
	1st	2nd	3rd	4th	5th	6th	7th	8th	9th	10th
RICC2 [eV]	0.717	1.086	1.328	1.544	1.709	–	–	–	–	–
f	–	–	–	–	–	–	–	–	–	–

Table A2.2: Higher excitation energies and associated oscillator strengths (f) of rhodopsin (SBH) Glu-113 different protonation states calculated at RICC2/cc-pVDZ and DFT/B3LYP level of theory.

NTNU

Norwegian University of
Science and Technology